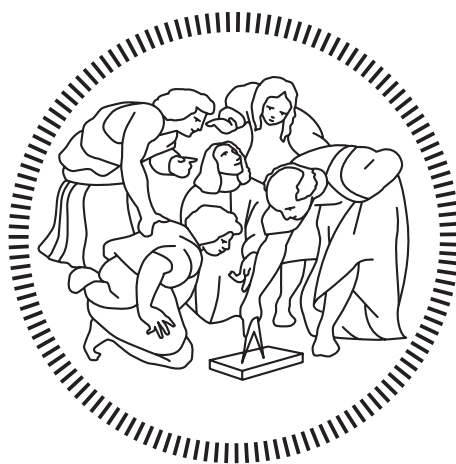# Politecnico di Milano

SCHOOL OF INDUSTRIAL AND INFORMATION ENGINEERING

Master of Science – Telecommunication Engineering

A Novel Tomographic Approach for an Early Detection of Multiple Myeloma Progression

Supervisor
Prof. Marco MARCON

Co-Supervisor
Ph.D. Marco Brando Mario PARACCHINI

Candidate
Andrea LEGGIO – 893760

Acknowledgements

Sommario

Mai come nell'ultimo anno l'uomo ha compreso l'importanza della ricerca in campo medico. Molte malattie rare a causa della loro bassa incidenza non hanno ricevuto una tecnologia adeguata e moderna a supporto, una di queste è il Mieloma Multiplo. Questa patologia copre l'1 % di tutti i casi di tumore e per questo ancora oggi i medici non dispongono di strumenti che possano facilitare e accelerare il processo di diagnosi e follow-up .

L'obiettivo di questo studio è quello di proporre moderne metodologie di Image Processing a supporto del medico per l'individuazione di decorsi su lesioni causate da Mieloma Multiplo, queste lesioni infatti sono la caratteristica più efficace per valutare il decorso della malattia così da guidare e sostenere il paziente in modo appropriato. I punti cardine di questa tesi sono quindi lo sviluppo di algoritmi avanzati capaci di semplificare il processo di diagnosi fino ad ora limitato dalla natura stessa dei processi adottati, tali processi sono delle analisi effettuate dall'operatore su ogni sezione del paziente visionando singolarmente ogni slice delle scansioni TC. Questo ovviamente provoca un'enorme richiesta di tempo con un risultato comunque limitato dall'occhio del medico e dal supporto visivo che adotta per il controllo delle TC. Gli algoritmi proposti sono quindi in grado di aumentare le capacità della valutazione offrendo la possibilità di identificare anche le più piccole variazioni altresì impossibili da notare con le attuali metodiche anche per l'occhio del medico più esperto.

Gli algoritmi sviluppati sono due, l'algoritmo di sezionamento e l'algoritmo di allineamento. Il primo ha un duplice scopo, quello di automatizzare il processo di selezione di specifiche parti del corpo dalle scansioni TC totali così da essere applicate all'algoritmo di allineamento e quello di supportare il processo di creazione di uno specifico set di dati sul mieloma multiplo per una futura applicazione di algoritmi basati su deep learning. Il secondo invece, l'algoritmo di allineamento, ha lo scopo di effettuare un perfetto allineamento tra i volumi ossei ottenuti da scansioni TC appartenenti allo stesso paziente ma effettuate in tempi diversi in modo da poterne effettuare il confronto e fornire informazioni visive sullo sviluppo delle lesioni causate dal Mieloma Multiplo. L'applicazione di questi algoritmi ha quindi confermato l'efficacia dei metodi proposti, infatti è stato possibile realizzare un processo di sezionamento automatico in grado di isolare volumi specifici in modo da poter essere forniti in input all'algoritmo di allineamento e produrre dati in grado di indicare se si è verificato un decorso della lesione e in che estensione.

Questi risultati pongono le basi per sviluppi futuri in quanto rappresentano sia un risultato applicativo già performante ma anche strumenti finalizzati allo sviluppo di un data set specifico da utilizzare per lo sviluppo di algoritmi automatici basati su deep learning per futuri studi e applicazioni relative al Mieloma Multiplo.

Abstract

The pivotal role of research in the medical field has been profoundly highlighted by recent events. Many rare diseases due to their low incidence have not received adequate and modern technology to support them, one of which is Multiple Myeloma. This pathology covers 1% of all cancer cases and for this reason doctors still do not have tools capable of facilitate and accelerate the diagnosis and follow-up process.

The aim of this study is to propose modern Image Processing methodologies to support the physician for the identification of courses on lesions caused by Multiple Myeloma, these lesions are in fact the most effective feature to evaluate the course of the disease so as to guide and support the patient appropriately. The key points of this thesis are therefore the development of advanced algorithms to simplify the diagnosis process which has been limited until now by the nature of the processes adopted. These processes consist in analysis carried out by the operator on each section of the patient, viewing each slice of the CT scans individually. This obviously causes an enormous investment of time with a result however limited by the doctor's eye and by the visual support he adopts for the control of CT scans. The proposed algorithms are therefore able to increase the resolution of the evaluation allowing the possibility of spotting even the smallest variations which could be impossible to notice with current methods even by the eye of the most experienced doctor.

The method developed in this work could be split in two main contributions, the sectioning algorithm and the alignment algorithm. The first has a dual purpose, to automate the process of selecting specific body parts from total CT scans to be applied to the alignment one and to support the process of creating a specific multiple myeloma dataset for a future application of deep learning based algorithms. The second algorithm, the alignment algorithm, has the purpose of making a perfect alignment between the bone volumes obtained from CT scans belonging to the same patient but carried out at different times in order to be able to compare them and provide visual information on the development of the lesions caused by Multiple Myeloma.

The application of these algorithms has therefore confirmed the effectiveness of the proposed methods, in fact it has been possible to create an automatic sectioning process capable of isolating specific bone volumes in order to be supplied as input to the alignment algorithm. We have succeeded in producing data able to indicate whether a course of the lesion has occurred and to what extent.

These results lay the foundations for future developments as they represent both an already performing application result but also tools aimed at developing a specific data set to be used for the development of automatic algorithms based on deep learning for future studies and applications related to Multiple Myeloma.

Contents

Contents

List of Figures

List of Tables

Chapter 1

Introduction

Nowadays, providing adequate technical support to medical personnel is a key point for timely and effective diagnosis. The presence of specific tools is essential to facilitate the process of diagnosis and control, tools that must be carefully modeled around the needs of doctors and the nature of the medical condition to be studied.

At present, only the trained and experienced eye of a specialist doctor can be relied upon to diagnose and monitor developments in patients with Multiple Myeloma. In fact, for this specific condition, described in more detail in Chapter 1.1, there are no specific tools as for other more common diseases and, unfortunately, problems can still arise for which making visual assessments accurately can be difficult even for an experienced doctor.

For a correct and in-depth diagnosis it is necessary to identify in the patient the bone lesions typical of Multiple Myeloma, lesions ranging from a size comparable to 1 mm to a larger area and which can affect substantial parts of the bone portion. Given the nature of these lesions, it is very difficult for a doctor to locate and correctly evaluate the evolution of these lesions over time, this comparison is a fundamental step to evaluate the course of the disease.

The method currently used by doctors it is shown in Figure 1.1 where the blue squares are the CT scans, in orange all the steps carried out by the doctor. It can be easily see that this workflow is mainly based on operations performed manually by the doctor himself, in fact the doctor after having acquired at different times two CT scans belonging to the same patient must check the different bone sections in each slice of the scan in search of lesions. Subsequently, the doctor has the task of reading the lesions belonging to the same bone sections of two different scans, the comparison must be performed in a meticulous way and relying only on the capabilities of the doctor's eye.

This process is obviously limited by several factors such as the experience and ability of the doctor who operates on the scans, the resolution of the visual support adopted and the size of the lesions that may be imperceptible to the human eye.

All these limitations are not only the cause of a final result that can be further improved, but also are the cause of the doctor's use of an enormous amount of time due to the repetitiveness of the process especially in high resolution scans. Furthermore, the process cannot be carried out by any doctor but only by specialized doctors with years of experience.
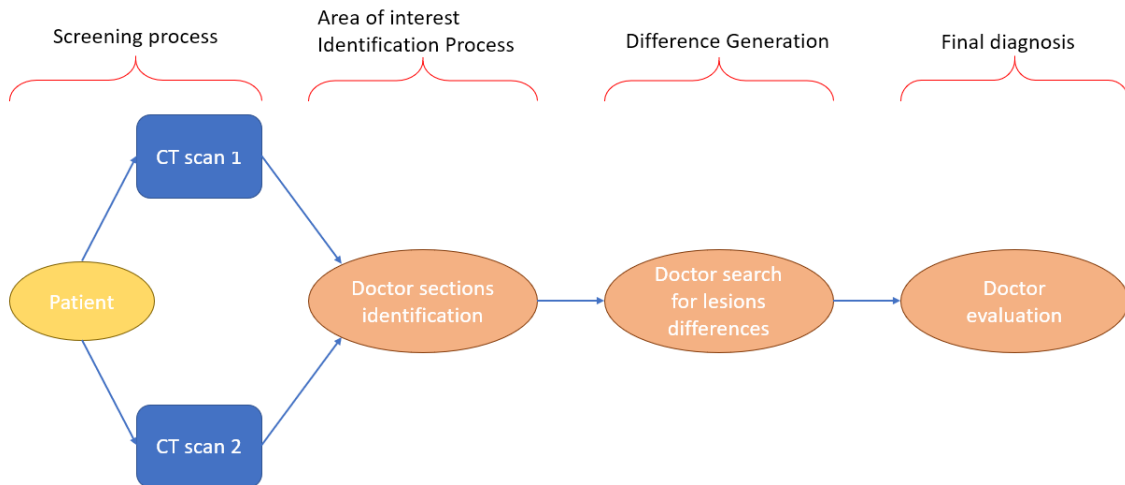
Figure 1.1. Workflow of the actual process for assessing Multiple Myeloma lesions course.

With these considerations, this thesis work was developed with the main purpose of providing the physician with image processing tools that facilitate and speed up the evaluation phases of the Multiple Myeloma course previously described.

These tools can be adopted by the physician to analyze and classify specific bone portions thanks to advanced automatic algorithms, so that the physician has at his disposal an easy-to-use tool capable of expanding and improving the capabilities and results of a process hitherto limited by the current image viewing tool but also by the manual nature of the method that must therefore be performed on each slice of each scan by the operator himself.

The Figure 1.2 shows the workflow and methods proposed in this thesis work in order to replace the current manual processes with advanced automatic processes so as to cover all the necessary steps. The blue squares represent CT scans or sub-volumes of them, the green ovals represents the automatic algorithms, the orange oval represent the part involving directly the doctor, the red oval represent tha usage of deep learning algorithms

Finally, an advantage in the application of the methods proposed in this thesis is the creation of data sets to support the future development of artificial intelligence methods based on deep learning. These applications can further improve the performance of the diagnoses, artificial intelligence and machine learning algorithms are revolutionizing and reinventing the world we know, including the medical field.

AI consists in the creation of intelligent behavior models on which a computer bases automated actions that require minimal human intervention. The models are based on algorithms able to self-learn and improve over time.

This "*intelligent automation*" allows to analyze data and make decisions very quickly, which is crucial in the medical field, especially in emergency and urgent situations.

The advantages of AI applied to medicine are of interest not only to medical staff, but also to patients. In fact, an efficient therapeutic model with *three actors* is introduced: the medical staff (1) who manages the tools enhanced by Artificial Intelligence (2) to assist and support the patient (3) along the path of therapy or treatment.
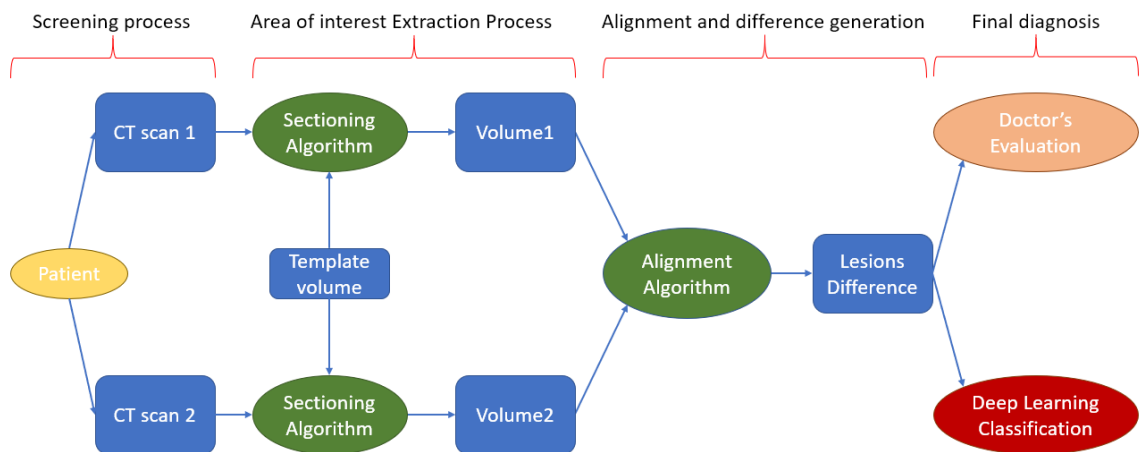
Figure 1.2. General process workflow proposed with this thesis work.

Here's how Artificial Intelligence optimizes healthcare:

- It allows doctors to save time and focus on the therapeutic process and patient care;

- Improves prognosis thanks to early diagnosis and immediate medical intervention;

- Promotes more accurate diagnoses, based solely on data analysis;

- It allows you to insert robotics systems within complex procedures or operations;

- Reduces unnecessary hospitalizations and hospitalizations;

- Reduces treatment costs thanks to a greater accuracy of the therapeutic approach;

- It favors new discoveries in the medical field, as a result of the analysis of huge amounts of data.

For the development of these advanced methods it is necessary to have a very large labeled dataset available to train and test the models. The extension of the data set is as important as the correct labeling, so the possible application of the developed methods can play a key role as it automates all those steps that would otherwise have to be done manually.

1.1 Introduction to Multiple Myeloma

Myeloma, also known as Multiple Myeloma, is a type of bone marrow cancer that originates from plasma cells, normally found in the bone marrow, which are cells that are part of the immune system.

Multiple Myeloma is a disease that accounts for 1% of all cancers and about 10% of hematological malignancies. It mainly affects adults and elderly people (average age of onset 60 years). Normal plasma cells produce antibodies (or immunoglobins) to help fight infections. In Myeloma, the abnormal plasma cells produce only one type of antibody known as paraprotein (Monoclonal Component or Component M), which does not perform any useful function, but whose dosage allows diagnosis and monitoring of Myeloma. In addition to producing Component M, plasma cells release a large amount of particular substances, called "cytokines", which through the stimulation or blocking of different cells can cause bone destruction, interfere with the production of bone marrow cells, including the production of red blood cells causing anemia, promote the growth of plasma cells at the expense of surrounding healthy cells. The bone marrow is the "spongy" material present in the central part of the largest bones of the body (see Figure 1.3).

Figure 1.3. Bone Marrow

In addition to being the site of origin of plasma cells, the bone marrow is the center for the production of blood cells (red blood cells, white blood cells and platelets). In Myeloma, because the DNA of a plasma cell is damaged, it transforms into a malignant or cancerous cell, known as a Myeloma cell. Unlike many cancers, Myeloma does not form a mass. On the contrary, Myeloma cells multiply and spread within the bone marrow. Myeloma affects parts of the body (hence the term Multiple Myeloma) where the bone marrow is normally active in an adult, for example, in the bones of the spine, skull, pelvis, rib cage, and areas around the shoulders and at the hips. The areas usually not affected are the extremities: hands, feet and the most distal parts of these. This aspect is very important as the functionality of these areas is preserved intact. Most medical problems related to Myeloma are caused by the accumulation of Myeloma cells in the bone marrow and the presence of paraprotein in the blood or urine. Common symptoms that occur in a patient with Myeloma are: bone pain (most often localized to the spine), bone fractures, fatigue (due to anemia), frequent

or recurrent infections (such as bacterial pneumonia, urinary tract infections and herpes zoster), renal insufficiency (often asymptomatic, it is discovered with blood tests without the patient presenting specific disorders) and hypercalcemia (which can give the patient drowsiness, muscle weakness, changes in the heart rhythm and constipation).

Some people may initially be diagnosed with MGUS (monoclonal gammapathy of uncertain significance), a benign condition, before developing Myeloma. The term indicates the presence of the abnormal protein (paraprotein) that is observed in the case of Myeloma, but the absence of other characteristic signs of the disease (less than 10% of plasma cells in the bone marrow and no evidence of bone disease). The risk of progression to active Myeloma from MGUS is very low: only 1% of patients for each year of observation of the disease. Although Myeloma cells are in higher numbers, between 10 and 30% of the total bone marrow, the growth rate can be very slow and represent the condition of silent or asymptomatic Myeloma. Both pathologies can change very slowly over the years and do not require any active treatment. It is very important to establish the correct diagnosis, distinguishing MGUS and silent Myeloma from active or symptomatic Myeloma, which instead requires therapeutic intervention. In recent years, we have seen new developments in Myeloma therapies and management that have significantly impacted how this disease is treated. Several studies are underway to develop new treatments and use existing ones better and more effectively. This guide illustrates and discusses many recently developed therapies in addition to existing ones. In addition to the treatment prescribed by the doctor, there are numerous measures that patients can take to improve the quality of life.

1.1.1   Types of Myeloma

Myeloma is often described as a disease that has individual characteristics, both in terms of complications reported by patients and in the way they respond to therapies, highlighting very significant differences. Some of these differences are due to the different types and subtypes of Myeloma. The diversity of Myeloma types and subtypes depends on the type of immunoglobin (paraprotein) produced by Myeloma cells. Each immunoglobin consists of a specific structure containing two main components: heavy chains and light chains. Inside the aforementioned components there are two heavy chains and two light chains (see Figure 1.4). There are five possible types of heavy chains defined by the letters G, A, D E and M and two possible types of light chains defined by the Greek letters kappa (κ) and lambda (λ).

Each individual immunoglobin (Ig) can only consist of one of the five possible types of heavy chain and only from one of the two types of light chain.

Most people with Myeloma, around 65%, are suffering from IgG type Myeloma, that is, Myeloma with immunoglobulin type G (one of five possible heavy chains) with kappa or lambda light chain component.

The other most common type of Myeloma is IgA type Myeloma with kappa or lambda light chains. Myelomas of type IgM, IgD and IgE are all quite rare. In addition to producing complete immunoglobins, 30% of patients it also produces at the same time isolated light chains (such as e.g. kappa light chains), detectable in urine or blood.

In about 20% of patients, Myeloma cells producelight chains only).

In this case we speak of "chain Myeloma light "or" Bence Jones "(BJ).
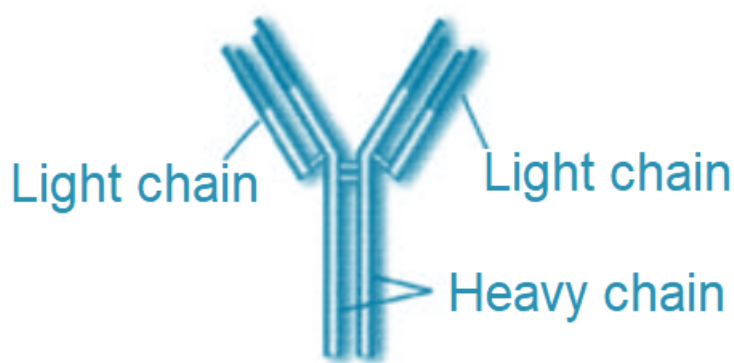
Figure 1.4. Immoglobulin structure

More rarely, in about 1-2% of cases, Myeloma cells produce very few or no immunoglobins at all; Yes therefore speaks of "non-secreting" Myeloma, making the diagnosis and monitoring very difficult. However, thanks to a recently developed test called the Freelite ™ test, it was possible to identify small amounts of light chains in most urine patients traditionally referred to as "non-secreting" patients, thus making diagnosis and monitoring easier. There are subtle differences between the different types of Myeloma. Like predictably, IgG Myeloma, which is the most widespread form, possesses all common features of Myeloma. On the other hand, sometimes the IgA type can be characterized by tumors outside the bones, while the IgD type can be accompanied by leukemia of the plasma cells and is more likely to cause kidney damage. Light chain or Bence Jones Myelomas involve a more likely to cause kidney damage and / or lead to deposits of light chains in the kidneys and / or nerves and other organs, resulting in a condition known as amyloid or light chains.

1.1.2 Multiple Myeloma's main causes

Although numerous studies have been conducted to identify possible causes of Myeloma, to date there are still no certain demonstrations.
It is believed that exposure to certain chemicals, smoking, high levels of pesticides, radiation, viruses and a weakened immune system (individual genetic trait), may be potential causes or triggers of the disease. It is likely that the Myeloma develops when a susceptible person has been exposed to one or more of the above factors. Since the onset of Myeloma is more common in old age, it is believed that this susceptibility may increase with the process of aging and consequent decrease in the functionality of the immune system, or that Myeloma may be the result of a accumulation of toxic insults or protracted antigenic exposures for long years.
Although unfamiliarity exists regarding the onset of Myeloma, the probability of it occurring is very low and there are currently no tests available that can predict this. Even when more than one case occurs in the same family of Myeloma, it is much more likely that the phenomenon is attributable to exposure to environmental factors rather than to the component hereditary.

1.1.3 Symptomatology

All medical problems related to Multiple Myeloma are caused by formation of malignant plasma cells and the monoclonal component. The consequences of this production are both local effects within the bone marrow where Myeloma cells are located, both extramedullary effects due to the M component, which is released into the circulation. The damage caused is classified with the abbreviation **"CRAB"** which indicates: Calcium, Renal, Anemia and Bone [1].

Myeloma cells release a whole series of cytokines which favor their adhesion at the level of the medullary environment; moreover they interfere with the bone remodeling process, where two types of cells that are normally in balance with each other participate: osteoclasts (which promote bone resorption) and osteoblasts (which instead produce constituents necessary for the formation of the bone matrix). The Myeloma cells will alter this balance, in favour of the activity of osteoclasts to the detriment of osteoblasts: what is obtained is bone damage with osteolytic lesions Fig.1.5; the bones most affected are the ribs, the pelvis and the spine while the areas that are usually not affected are the extremities i.e. the bones of the hands, feet, lower regions of the arms and legs.

Figure 1.5. 3d view of the patient's humerus with visible lesions

Therefore the bones become more fragile and can fracture even in the absence of trauma or more frequently with minor trauma this is know us as a pathological fract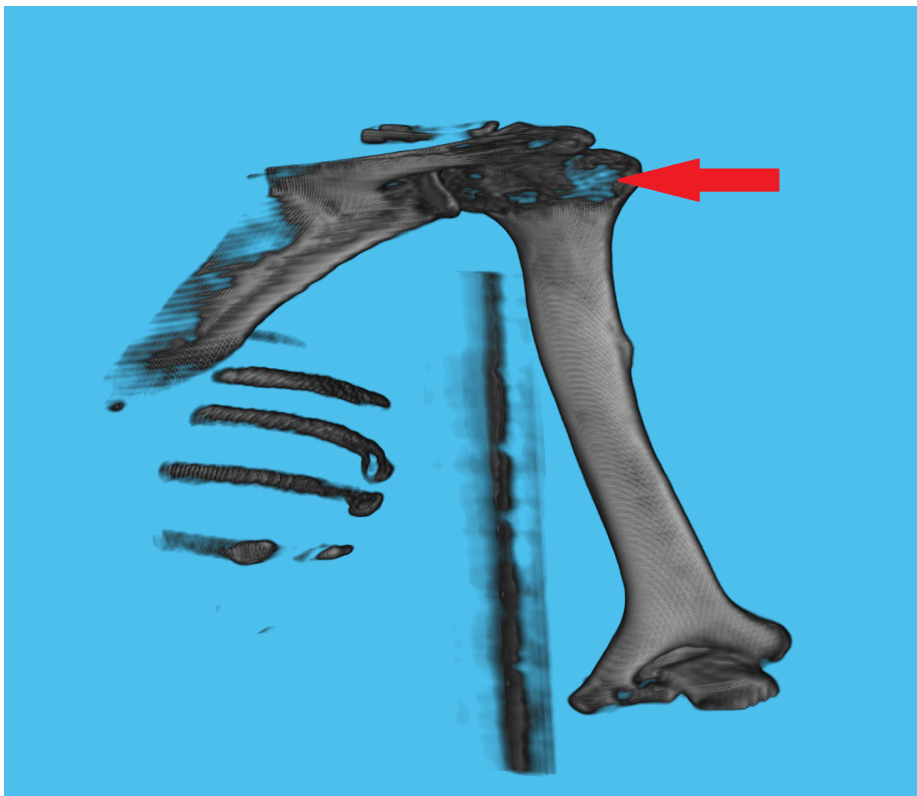ure. The bone destruction involves another consequence, the progressive loss of the mineral portion of the bone resulting in a large amount of calcium released into the blood causing hypercalcemia.

A third problem due to the presence of malignant cells in the bone marrow is the reduction of the function of the bone marrow in producing blood cells, i.e. red blood cells, white blood cells and platelets: consequences of a decreased production are: anemia (decrease in red blood cells), leukopenia (decrease in white blood cells) and thrombocytopenia (decrease in platelets). Moreover, the M component released by Myeloma cells into the blood can reach the kidney, altering and reducing the filtration capacity of the kidney: therefore the M component will pass into the urine forming the so-called Bence-Jones proteinuria.

Despite the presence of these problems, Multiple Myeloma often remains asymptomatic in the early stages and is perhaps discovered through a routine blood test showing a higher concentration of protein; otherwise it manifests itself with some symptoms which, however, are not specific symptoms that immediately link to the diagnosis of this pathology: therefore it is often diagnosed at an advanced stage. Initially, the first symptom that occurs in 70% of patients is bone pain especially in the lumbar and dorsal spine or in the hips; in 30% of patients, bone pain is accompanied by spontaneous pathological fractures (an example is vertebral compression fractures which can cause decreased muscle strength and a sense of tingling and numbness in the lower limbs, i.e. so-called paresthesias) [2].

The deficiency in the production of blood cells manifests itself in different ways: anemia is generally associated with a feeling of general sickness (tiredness and weakness) with lacking of breath and dizziness; thrombocytopenia is manifested by serious bleeding following small cuts, scrapes or bruises or with abnormal bleeding (from the nose or gums); leukopenia and the lack of functional antibodies capable of protecting our body from pathogens, manifests itself with an increased risk of infections and there is a greater manifestation of repeated colds, cough, bladder and kidney infection, the appearance herpes zoster and pneumonia.

Hypercalcemia is partially responsible for kidney damage, plus it can break the normal balance between electrolytes, with negative consequences both in the brain (mental confusion and difficulty in thinking) and in other organs, causing nausea, loss of appetite, dehydration, fatigue, weakness. Kidney damage can occur immediately, but very often it appears in further stages, during the progression of the disease, due to the accumulation of the monoclonal component in the blood and calcium released from the bones: thus there is a slower circulation, mental confusion and a decreased filtration capacity; if the M protein is able to pass the renal filter it can accumulate in the urine, leading to an increased concentration of protein in the urine (Bence-Jones proteinuria). Other type of changes are fever (as an initial symptom, but it is rare), venous thrombosis induced by a hyperviscosity of the blood or blood hyperviscosity syndrome (caused by an excess of monoclonal component in the blood) and peripheral neuropathy (the most frequent the carpal tunnel).

1.1.4 Diagnosis

Diagnosing Multiple Myeloma is not an easy task, precisely because many patients have no symptoms up to an advanced stage or present only generic symptoms which could be caused by other diseases. However, in an elderly patient with low back pain or bone pain, associated with fatigue and weakness, present for several weeks

Figure 1.6. 2d view from the z axis of the patient's humerus with visible lesions

despite symptomatic painkilling treatment, he must prompt the doctor to undertake diagnostic evaluations to check for the presence of more serious diseases including Multiple Myeloma [2]. Therefore, the doctor first of all carries out to the patient classical primary tests, i.e. blood tests and urinalysis in order to check the general state of health and renal functioning: on the blood sample CBC (Complete Blood Count) and blood chemistry tests (important for assessing creatinine, albumin and calcium levels) are required. Subsequently, more specific tests are required to verify the presence of the monoclonal protein of Myeloma: electrophoresis of serum and urinary proteins is done to evaluate the amount of Myeloma proteins present, followed by an immunofixation test to demonstrate the exact type of altered immunoglobulin . In the blood sample is also searched the presence of Beta-2-microglobulin, a protein produced by the malignant cells of Myeloma: this in itself it does not cause particular

problems, but calculating the quantity is useful for evaluating how advanced the cancer is; the level of this protein is therefore a tumor marker and gives clues to the aggressiveness of the tumor. If these tests reveal the presence of the monoclonal component in high quantities (greater than 3 g / dl), it is necessary to take a small sample of bone marrow blood (bone marrow aspirate) and a bone fragment to be biopsied: for the collection, a local anesthesia is administered through the skin above the sampling point (sternum or iliac bone). [2]. The samples will be analyzed to determine the number of malignant plasma cells within the bone marrow: in Multiple Myeloma the percentage of plasma cells exceeds 30% in the bone marrow.

Other tests can then be performed on the bone marrow sample [3]:

- Immunohistochemistry: technique that uses special antibodies that attack only a specific type of cell; their binding causes color changes, which can be observed under a microscope: this test is useful for finding and identifying the types of Myeloma cells.

- Flow cytometry: test similar to immunohistochemistry, which allows to identify the presence of abnormal cells and to identify their type. Special antibodies are used which will bind to cells only if a certain substance is present on the surface of these cells; these cells are passed in front of a laser beam and if the cells are bound by antibodies, the laser will cause them to emit a light that can be analyzed and measured by a computer.

- Cytogenetic examination: this test allows doctors to evaluate changes in the chromosomal structure in Myeloma cells, compared to normal bone marrow cells: the sample is observed under a microscope to verify these changes such as translocations, deletions, etc. Finding these alterations can help to estimate the patient's prognosis. The results of this test do they get it after 2-3 weeks because the cells have to grow on plates in the lab for a couple of weeks so they are ready to be analyzed.

- FISH (**F**luorescent **I**n **S**itu **H**ybridization): technique similar to cytogenetic examination and fluorescent dyes are used that attack only specific parts of chromosomes. It is a technique that can find even smaller chromosomal changes, so it is a more accurate test, plus the results are obtained in a few days because growth in the laboratory is not necessary.

- Imaging tests and documentation: with this kind of information it is possible to assess the presence, severity and location of bone lesions:

  1. X-ray of the skeleton: This exam mainly involves x-rays of the skull, spine, humerus, ribs, femur and pelvis (i.e. the bones most frequently affected by injuries and fractures). Bone damage appears in the form of "spots" or "holes"; it is not immediately visible in all patients, but can be observed after a 50% loss of bone.

  2. Magnetic Resonance: technique that allows us to obtain a more detailed image than radiography; it is used when x-rays show no lesions but the patient still has bone pain. It therefore serves to reveal the presence and

distribution of the disease in the bone marrow and, in addition, it can be useful when spinal compression is suspected.

3. Computed tomography (also commonly called CT): used when the x-rays are negative or to obtain more detailed images. Instead of obtaining a single image, as in radiography, with the CT scan multiple figures of the part of the body being analyzed are obtained. All these 'slices' will be combined into a single 3d-image so as to have a more detailed evaluation. The CT scan can also be useful to perform a biopsy and therefore identify the precise point where to perform it.

4. Positron Emission Tomography (PET): more sensitive diagnostic technique for evaluating the interior of the organism; it is not a standard exam, but is used for patient staging and follow-up.

All these imaging techniques are essential for the doctor who will be able to accurately assess the location and extent of bone damage caused by Multiple Myeloma

Among all the methodologies for Multiple Myeloma diagnosis, the visual one through the use of a CT scan it is currently the most effective and therefore the most important. In fact, the presence of bone lesions is a characteristic symptom of the disease while other data that can be evaluated by other types of analyzes may be caused by other pathologies.

The method currently used to diagnose Multiple Myeloma, is mainly based on operations performed manually on CT scans, this Biomedical Imaging method ranks as one of the top five medical developments in the last 50 years, according to most medical surveys. CT has proven so valuable as a medical diagnostic tool that the 1979 Nobel Prize in Medicine was awarded to the inventors. Both CT and conventional x-rays take pictures of internal body structures. In conventional x-rays, the structures overlap. For example, the ribs overlay the lung and heart. In an x-ray, structures of medical concern are often obscured by other organs or bones, making diagnosis difficult. In a CT image, overlapping structures are eliminated, making the internal anatomy more apparent.

During CT imaging, an x-ray tube rotates around the patient so that multiple images are collected from many angles. These images are stored in a computer that analyzes them to create a new image with the overlying structures removed. CT images allow radiologists and other physicians to identify internal structures and see their shape, size, density, and texture. This detailed information can be used to determine if there is a medical problem, provide the extent and exact location of the problem, and reveal other important details that can help the physician determine the best treatment. The images may also show if no abnormality is present. A CT scan that shows no abnormality still provides useful data.

The information aids the health care provider by focusing attention away from unnecessary medical concerns. Modern CT scanners acquire this information in seconds, sometimes in fractions of a second, depending on the examination. Benefits of CT include more effective medical management by determining when surgeries are necessary, reducing the need for exploratory surgeries, improving cancer diagnosis and treatment reducing the length of hospitalizations, guiding treatment of common conditions such

as injury, cardiac disease and stroke improving patient placement into appropriate areas of care, such as intensive care units.

CT scanning provides medical information that is different from other imaging examinations, such as ultrasound, MRI, SPECT, PET or nuclear medicine. Each imaging technique has advantages and limitations. The principal advantages of CT are its abilities to rapidly acquire images, provide clear and specific information, image a small portion or all the body during the same examination.

No other imaging procedure combines these advantages into a single session.

To assess Multiple Myeloma lesions nowadays doctors must check each slice of the CT scan for each boy part in search of lesions. Subsequently, in follow-up phases, the doctor has the task of checking new CT scans of the patient carried out after one or more years. In these phases, after having identified the lesions previously noted in the medical report, the physician must visually compare each lesion slice by slice to assess whether these have undergone changes with consequent extension of bone absorption. This process is obviously limited by several factors such as the experience and ability of the doctor who operates on the scans, the resolution of the visual support adopted and the size of the lesions that may be imperceptible to the human eye.

Another limitation that arises with current methods is due to the machinery used by the doctor and its ordinary replacement, in fact many institutes update their machinery frequently and this does not only involve a difficulty due to the fact that the doctor must learn the use of a new machine, but also and above all by the fact that the output provided by the machine has different characteristics as regards the display support. Current machines to perform CT scans offer different views of the acquired data in terms of image processing of the data, these differences are of great impact for the visual evaluation of the doctor who, when replacing the machine used for a long period, must retrain the their ability to search for lesions by adapting to the characteristics of the new support.

Furthermore, the possibility of evaluating the lesions with advanced algorithms, capable of discerning even the smallest spatial characteristics, and the ability to check the evolution of these lesions is a game changer feature as it could help the doctor to find lesions that would be impossible to find with the naked eye in diagnosis process which is a crucial moment.

1.1.5 Thesis Structure

- **Chapter 2** reports the **State of the Art** of biomedical imaging methods as well as the state of the art of the algorithms used.

- **Chapter 3** introduces and describes the developed **Methods**. In the initial part of this chapter, section 3.1, data analysis and adopted preprocessing are described starting from data provided by the National Cancer Institute (INT) which were analyzed and its structure and specific format of the biomedical imaging file were studied. Then the main methods developed are discussed, these are the Sectioning Algorithm and the Alignment Algorithm. The Sectioning Algorithm 3.2 is a method which has the the goal of identifying and extracting specific parts of the body from a general volume. The Alignment Algorithm, presented in section 3.3 is an algorithm whose goal is that of aligning two volumes extracted by the Sectioning Algorithm containing the same bone portions acquired from different scans obtained in different periods in order to compare them and highlight their difference.

- **Chapter 4** reports the most significant **Results** on various use cases developed of the previously mentioned methods.

- **Chapter 5** reports the **Conclusions** of this work and potential paths for future works are described.

Chapter 2

State of The Art

2.1 Main Methods of Biomedical Imaging

In recent years there has been a real explosion of new acquisition techniques of images representing the most diverse aspects of human anantomy and possible pathologies connected to them. Each type of acquisition is referred to as "Imaging Methods" . Some modalities have become in common use and their impact on clinical practice and diagnostic has been extensively validated.

For others, however, it cannot yet be considered completed the phase of clinical/diagnostic validation, other than the development of algorithms that make the information acquired or produced on a large scale more easily accessible visually, or scale at low cost so that most medical facilities can have access to this technology.

Generally, the methods for acquiring medical images can be divided in two main categories: on the one hand there are structural images (anatomical imaging) characterized by High Resolution (think, for example, Computed Tomography (CT) and Magnetic Resonance Imaging (MR)) and used to describe anatomical morphology. On the other hand there are the functional images, with Low Resolution (PET, SPECT or fMRI), to study the metabolic functionality associated with anatomical structures. Biomedical imaging provides non-invasive diagnostic means, which provide information on the internal parts of the bodies. Theirs functioning is based on the different behavior of the atoms, contained in the bodies, when they are subjected to external stresses, or rather when they absorb energy. Among the imaging modalities on which the research activity is focusing in medical image analysis there are the following.

2.1.1 Computed Tomography

Computed tomography (CT) was the first fully digital imaging technique.

In the early 1970s, Godfrey N. Hounsfield designed and built the first CT device, revolutionizing medical diagnostics. He was awarded the Nobel Prize for Medicine in 1979, with Allan M. Cormack, who in previous years had defined the theoretical basis for the reconstruction of tomographic images. CT is also referred to as CT (Computed Axial Tomography) as it produces images of transverse or axial layers of the body.

The CT device is equipped with an X-ray tube that rotates around the patient emitting X-rays which, after passing through the body, are intercepted by solid or gas-state detectors (detectors). In this way, multiple projections of sections of the body are

obtained, i.e. X-ray attenuation data from different points of view.

Like radiography, CT obtains transmission images. However, unlike radiography, CT obtains measurements of tissue densities and, thanks to the tomographic representation and greater contrast, highlights structures not visible on radiography. The CT image is reconstructed with mathematical algorithms that require complex calculations that can be quickly achieved only by a computer. The reconstruction algorithms are of the iterative or analytical type. The former calculate the densities of the voxels with a series of hypotheses and checks of the values based on the measured data: the higher the number of iterations (repetitions), the more accurate the calculations. An iterative algorithm was used by the first CT apparatus; subsequently, the fastest analytical algorithms based on the preliminary processing of the acquired data were introduced, followed by the rear projection in the final image (FBP, Filtered back projection).
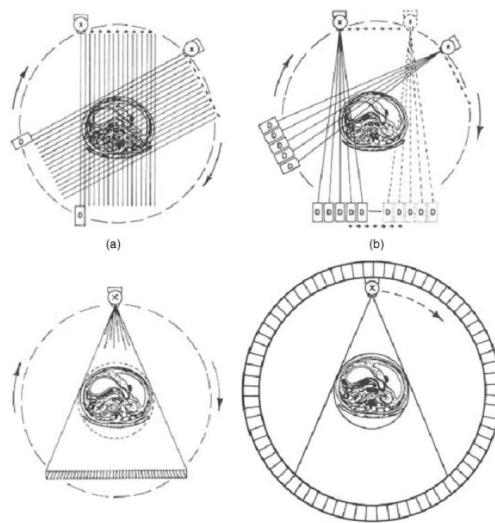
Figure 2.1. Examples of CT scan

CT apparatuses were progressively equipped with more advanced X-ray tubes and more numerous and efficient detectors. At the beginning of the nineties, the first CT devices with helical scanning (helical spiral CT) were introduced, which allow the acquisition of data during a continuous rotation of the X-ray tube-detector complex, with simultaneous advancement of the patient bed. The examination time has been significantly reduced with multisection (multilayer) spiral CT, which can now acquire up to 256 data sets (i.e. body layers) simultaneously.

Today, the study of the whole body of an adult can be performed in less than a minute, while a CT study of the skull alone with the first CT devices required more than an hour. The reduction of the dimensions of the detectors allows to obtain thin layers and above all voxels of cubic shape (i.e.of equal dimensions in all directions, isotropic voxels). This allows for spectacular three-dimensional reconstructions. The extraordinary 3D anatomical representation of skeletal structures, heart (cardio-CT) and vascular structures (angio-CT) is of considerable impact in multisection CT. CT data, as well as for diagnostic purposes, are useful for planning surgical therapy and radiotherapy.
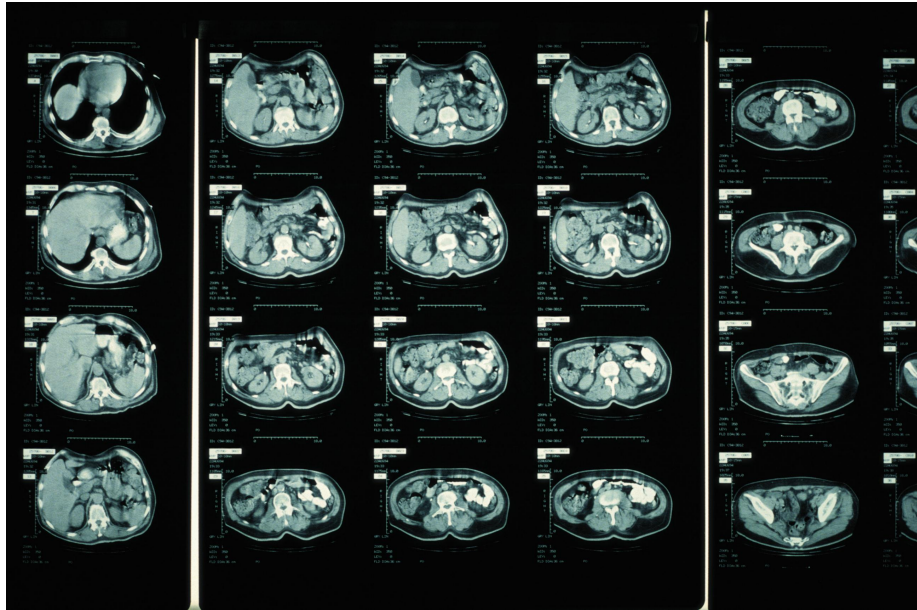
Figure 2.2. CT Scan Example with different slices representing a 3d volume

2.1.2 Other Imaging Methods

Radiodiagnostics (radiography and radioscopy)

Radiography is the two-dimensional representation of a structure crossed by X-rays, some of which are stopped or deflected (attenuated). The denser and thicker the structure, the more likely the rays are attenuated. The X-rays that pass through the body intercepting a sensitive target determine the formation of an image, which reflects the density and thickness of the structures under examination. In the conventional radiographic technique the X-ray target is a photographic film placed in a container (radiographic cassette) which protects it from exposure to light and which contains reinforcement screens, fluorescent panels capable of enhancing the effect of the rays by reducing their quantity. needed to produce the image.

The visualization of radiographic images on film requires a chemical treatment (development) similar to the photographic one, after which the denser structures, such as bones, are displayed in white / light gray, while those less dense, which contain air such as lungs, have dark shades. After development, the no longer editable image can be analyzed on a backlit surface (diaphanoscope or negativoscope).

In the radioscopic technique, the X-ray target is a screen of fluorescent material which gives real-time images of the structures under examination. Radioscopy is used, among other things, to identify the areas on which to perform radiographs, to guide the execution of biopsies and the placement of catheters, to monitor surgical interventions, and also to evaluate the functionality of the digestive tract.

Radiography and radioscopy visualize structures that contain high (bone) or low density (air / gas) materials well, but are not very effective for the study of soft tissue of intermediate density. But the natural ability of body structures to attenuate X-rays can be increased or decreased by administering high and / or low density materials (contrast media or contrast medium). These materials, to the development of which pharmaceutical research has made a great contribution, help to visualize

Figure 2.3. Radiography Examples

structures that are not directly or at all visible and are used above all to study blood vessels (with the investigation called angiography), the urinary and digestive systems. . Contrast media with different chemical characteristics are routinely used to increase diagnostic information also in CT and MRI and, less frequently, in ultrasound.

In the last twenty years, computer advances and the development of new materials sensitive to X-rays have allowed the birth and diffusion of digital radiology, which is achieved with approaches essentially attributable to two categories: Computed radiography (CR) and Direct digital radiography (GDR).

CR with photo-stimulable phosphor computed radiography (PPCR) that capture X-ray energy and can be analyzed with light radiation, has been widely used, as it uses devices that can be incorporated into containers similar to radiographic cassettes traditional. CR can therefore be performed with all conventional radiographic equipment. DDR more expensive but faster than PPCR, uses panels of selenium or amorphous silicon, integrated into the X-ray table and connected to a reading device that allows immediate transmission of data to monitors and PACS.

Digital radiology has biological and environmental advantages, as: (a) it reduces the cases that require repetition of the examination and, consequently, decreases the overall dose of rays to patients; (b) eliminates the chemical treatment procedures of the films and the consequent production of toxic waste. Digital images are typically studied on monitors where they can be processed and analyzed in detail.

Densitometry (computerized bone mineralometry)

Densitometry (DXA, Dual energy X-ray absorptiometry) is the radiographic derivation technique that allows you to measure the mineral content of the body. By measuring the absorption of X-rays of two different energies, it is in fact possible to obtain data such as: (a) BMC (Bone mineral content); (b) BMD (Bone mineral density); (c) fat mass and lean body mass. The examination, which is performed on the whole body or on body segments (limbs, spine), is indicated for the diagnosis of osteoporosis and osteopenia. Osteoporosis is more common in postmenopausal women and involves an increased risk of fractures. Due to the possibility of measuring fat and lean

mass, densitometry can also be used to monitor dysmetabolic diseases diet programs in particular situations (eg, anorexia, obesity). Even with CT, if the X-ray tube can produce X-rays of two different energies, it is possible to perform bone density measurements (usually limited to the vertebrae).

Nuclear Medicine

Nuclear medicine studies the diagnostic (imaging and laboratory) and therapeutic (metabolic radiotherapy) applications of radioactive atoms (radionuclides). The fundamentals of the discipline are linked to the discovery of radioactivity and the production of artificial radionuclides with particle accelerators such as the cyclotron (built in 1931 by Ernest O. Lawrence).

In nuclear medical imaging, molecules defined as radiopharmaceuticals (without any pharmacological effects), labeled with γ-ray emitting radionuclides, are administered (usually intravenously). Then, with equipment such as γ cameras, images of the distribution of radiopharmaceuticals that reflect biological functions are obtained.

The nuclear-medical image is of the emissive type because the patient is the source of the signal. The γ rays are detected by scintillation detectors consisting of NaI [Tl] (sodium iodide with thallium impurities) or other materials capable of emitting flashes of light (scintillations) when they intercept the γ rays. The name scintigraphy for nuclear-medical investigations derives from the scintillations.

Different organs and functions are studied with different radiopharmaceuticals. For thyroid scintigraphy that produces iodinated hormones, for example, it is possible to administer radioactive iodine or other radioactive anions such as 99mTcO4 (pertechnetate) that can be taken up by thyroid cells. With the aid of computers, scintigraphic examinations can measure tissue functions, based on the knowledge of the biodistribution mechanism of the radiopharmaceutical used and the availability of a mathematical model that describes its distribution. The radiopharmaceuticals used in quantitative functional analyzes are defined tracers (of biological functions) and the set of knowledge underlying the quantitative studies is the theory of tracers. Among the most widespread quantitative analyzes in clinical practice are the measurement of glomerular filtration and renal plasma flow with renal scintigraphy and the measurement of cardiac output and the ejection fraction of the left heart ventricle, with angiocardioscintigraphy. Functional data can be presented as parametric images, in which the grayscale or color scale displays the different levels of the studied parameter. Example of a parametric image is the phase map of cardiac contraction obtained with angiocardioscintigraphy, in which the heart walls that contract synchronously (in phase) are displayed with the same color, while the areas that do not move in synchrony (dyskinetic or akinetic) have a different color. In nuclear medical imaging, radionuclides are used with short radioactivity halving times (usually minutes or hours). The 99mTc (Metastable Technetium99, γ-ray emitter) and the 18F (Fluorine-18) positron emitter are the most used.

The main instrumental evolution of nuclear-medical imaging has been the development of tomographic techniques (**SPECT** and **PET**). **SPECT** uses the radionuclides used in traditional scintigraphy (such as 99mTc), and ad hoc devices or, more often, rotating gamma cameras, which can acquire data from different points of view, necessary for the reconstruction of tomographic images. **PET**, on the other hand, uses positron-

emitting radionuclides (positively charged particles which, interacting with electrons in a process called annihilation, transform into pairs of γ rays) and devices with a similar appearance and size to those of CT, equipped with surround the part of the body under examination.
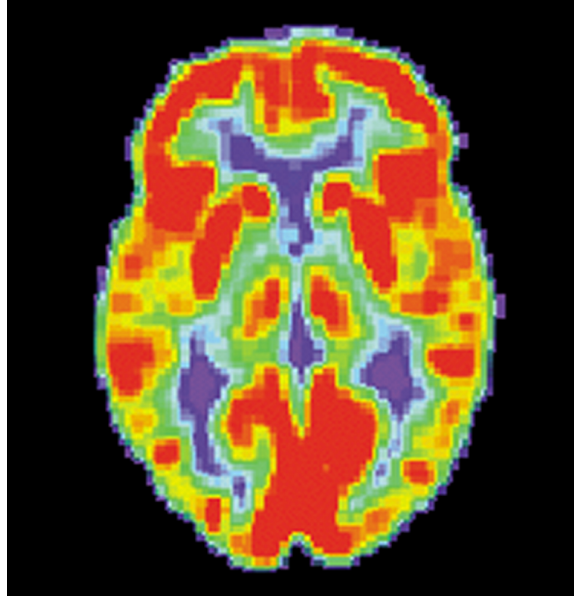
Figure 2.4. PET brain image

Positron-emitting radionuclides decay rapidly and are usually produced by cyclotrons placed near the PET device. PET is a relatively complex and expensive technology that allows accurate measurements of tissue radioactivity, and is the most powerful molecular imaging technique today.

PET investigations have wide application in oncology for biological characterization, staging (extent assessment) and tumor monitoring. A glucose analogue radiopharmaceutical, [18F] -fluorodeoxyglucose (FDG) is mainly used in these tests. Since malignant tumor cells uptake more glucose than normal ones, PET-FDG studies highlight tumors that uptake more glucose in proportion to their malignancy and can evaluate the effectiveness of ongoing therapies, which is generally associated with a reduction in accumulation of glucose.

The consumption of glucose is only one of the evaluable functions. Blood flow, protein and lipid metabolism, oxygen consumption, DNA synthesis are studied with other radiopharmaceuticals; molecular markers (antigens, receptors) can also be identified and neurotransmission processes examined. Furthermore, PET can be used in pharmaceutical and preclinical research to study the body distribution and functional effects of new drugs, and advanced gene therapy applications.

PET has also clinical use in cardiology for the study of ischemic heart disease and in neurology, for the characterization of neurodegenerative diseases, such as Alzheimer's and Parkinson's, and for epilepsy.

An important technological advance has been the development of hybrid devices in which PET and SPECT are integrated with CT systems; it is thus possible to perform CT and functional SPECT or PET morphological examinations in the same session, accurately locating the functional activities investigated with SPECT and

PET. Hybrid PET-MRI appliances are also in advanced development.

Magnetic Resonance Imaging (MRI)

The phenomenon of nuclear magnetic resonance (NMR, Nuclear magnetic resonance) discovered in 1944 by Felix Bloch and Edward M. Purcell (Nobel Prize winners in Physics in 1952) is the basis of one of the major advances in imaging since the discovery of X-rays . NMR occurs only in the presence of high intensity magnetic fields (thousands of times higher than Earth's), in atomic nuclei with odd number of protons and / or neutrons. Different nuclei have different resonance frequencies, according to the Larmor equation: $\omega = \gamma H_0$ where ω is the resonant angular frequency, H_0 is the intensity of the magnetic field and γ is the gyromagnetic ratio, a constant characteristic of each nucleus. Resonance (nuclear excitation) is obtained with oscillating magnetic fields, created by electrical circuits (coils), at the resonant frequency of the nuclei to be studied, and is characterized by minimal variations in nuclear energy levels that do not cause molecular modifications. The techniques based on this phenomenon are non-invasive for biological structures and do not expose the patient to ionizing radiation. Magnetic resonance imaging (MRI) devices use superconducting or permanent magnets and, to obtain images, excite the nuclei of the hydrogen atoms of water molecules, the most abundant chemical species in the body. Once the excitation is over, the nuclei relax, releasing the acquired energy, inducing weak electric currents in the device circuits whose analysis allows the reconstruction of the images. For the localization (spatial coding) of the signal, circuits (gradients) are used, which gradually vary the intensity of the main field so that the voxels have slightly different resonant frequencies. With MRI scans are obtained in all possible spatial directions, without changing the patient's position and it is possible to acquire data in 3D mode.

An axial MRI looks at the brain from below in a series of images starting at the chin and moving to the top of the head.

A sagittal MRI looks at the brain from the side in a series of images starting at one ear and moving to the other.

A coronal MRI looks at the brain from behind in a series of images starting at the back of the head and moving to the face.
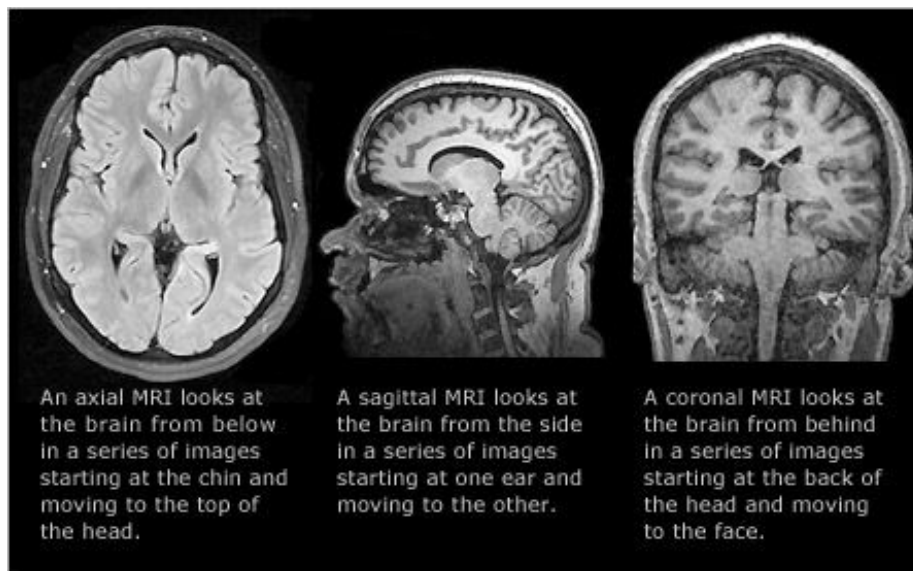
Figure 2.5. Typical magnetic resonance images of the brain. From left to right, it is respectively shown the axial, sagittal and coronal reconstruction

Several physical phenomena influence the relaxation of nuclei and the resulting signal. In MRI images can be created weighted on different parameters, such as T1 relaxation time (spin-lattice), T2 relaxation time (spin-spin), proton density, magnetic susceptibility and molecular diffusion (Brownian motions) . The MRI signal is also influenced by blood flow, the presence of ferromagnetic materials, and changes in the vascular concentration of oxy- and deoxyhemoglobin which can act as markers of tissue perfusion. The analysis of diffusion and perfusion phenomena allows the study of functional aspects especially in the nervous system (fMRI, functional MRI) for research applications in cognitive neuroscience, and for diagnostic use in neurology and psychiatry.

Since the introduction of the first commercial devices in the 1980s, the applications of MRI have continually increased. With the improvement of hardware (magnets with higher fields, better circuits, faster computers) and software (pulse sequences, data processing), high-detail images of all anatomical structures are obtained, with excellent results for the system central nervous system and the musculoskeletal system but also for the heart and abdominal organs. The high contrast and multiparametric characteristics are very useful for tissue classification procedures, necessary for measuring the volumes of normal and pathological structures (morphometry).

In research and diagnostic applications, MR spectroscopy (MRS, Magnetic resonance spectroscopy), used in chemistry well before the introduction of MR imaging, also plays an important role. Chemical analyzes with MRS are possible because each nucleus has a slightly different resonance frequency depending on the shielding of the main magnetic field by the surrounding electrons; therefore nuclei of the same atom in different molecular positions have slightly different resonance frequencies. By processing MRS data it is possible to create spectra whose peaks correspond to specific molecules. MRS can be applied to stable nuclei of biological interest (1H, 31P, 13C, 19F) and, with high intensity magnets, can contribute to the *in vivo* molecular characterization of various diseases - in particular tumors and diseases of the nervous system. central - forming an integral part of molecular imaging.

2.2   Co-Registration definition and base concepts

Both *Sectioning Algorithm* and *Alignment Algorithm* further discussed in Chapter 3 are based on the co-registration process. The term image co-registration refers to the process of estimating a *optimal spatial transformation* that allows to superimpose two or more images of the same scene taken at different times, from different points of view or with different sensors [4].

In other words, the goal of a co-registration algorithm is to determine the spatial transformation which maps the points of an image to the corresponding points of the image we want co-register as schematically shown in Figure 2.6.

In the context of Computational Vision, co-registration is a widely used technique used for many applications including, for example, creating panoramic images [5], remote sensing [6], microscopy [7], robotics [8] and, obviously, the medical imaging area. In general, beyond the specific objective pursued in the particular application,
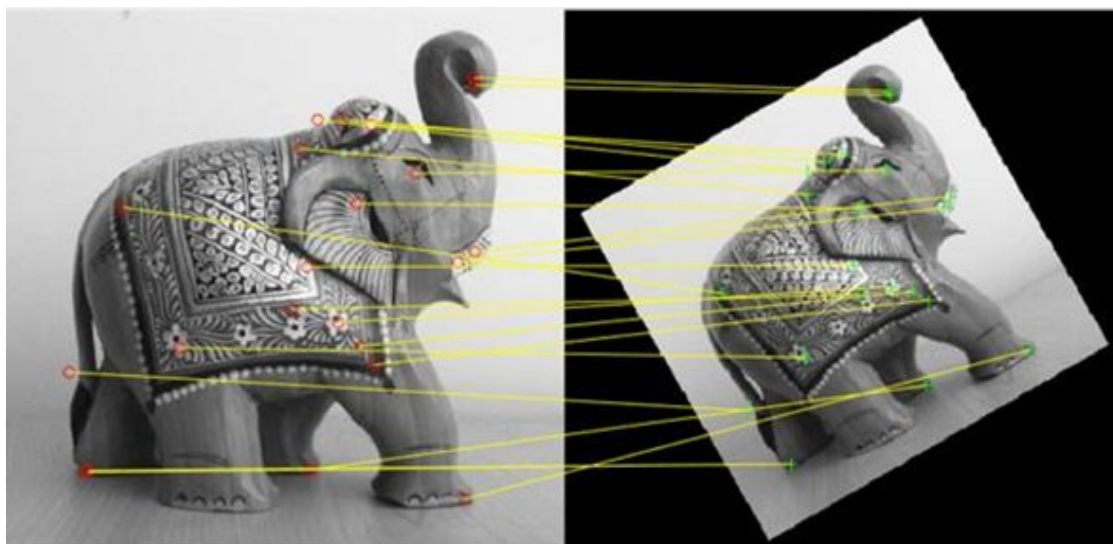
Figure 2.6. Image Registration

it is possible to group the different co-registration algorithms according to how they capture the input images.

Therefore, we have optimized algorithms to work on pairs of images depicting the same scene but acquired:

- from different points of view (multi-view analysis)

- at different times (multi-temporal analysis)

- through different types of sensors (multi-modal analysis)

Finally, it is important to remember a fourth category, in which we try to co-register an image with a synthetic model (atlas-based analysis).

For the diversity of the images to be co-registered and for the multiple situations where co-registration is required, there is no (and probably cannot be) a universal method applicable at all circumstances. What we have witnessed, therefore, is the affirmation of different methods, each of which proved to be efficient in a specific area.

Such methods differ in some fundamental architectural and algorithmic choices.
For example, a first distinctive element concerns the type of *geometric deformation* between the images that we try to estimate; other elements are the *similarity* measure used to determine how much close to the expected result, the *interpolation technique* to assign a value to the image pixels which, following the transformation, do not appear to belong to the bi or three-dimensional output image grid. Finally, the choice of the method of exploration of the parameter space during the estimation of the optimal ones(which is associated with the desired co-registration transformation) is crucial.

In order to find one's way within this possible infinite range of solutions, the following breakdown it has become standard into distinct sub-problems of co-registration:

- Estimate of the transformation

- Measure of the distance (called metric) between images

- Interpolation

- Optimization

All co-registration algorithms are distinguished from each other by the particular solution used to solve the four previous sub-problems. These choices are made basing on the particular mode of acquisition of the pair of images, the type of noise e the desired accuracy in estimating the optimal transformation.

To properly summarize the previous subdivision, the algorithmic flow of a generic co-registration method is represented schematically in Figure 2.7. The literature refers to the two input images to be co-registered as a reference image (the one between the two that remains fixed) and template image (i.e. the one on which the transformation is applied). This task can be deal both with bidimensional data (images) or three dimensional data (volumes/voxels). In Figure 2.7, the Transformation block represents the transformation of the points from space of the fixed image to that of the movable image. Metrics is a measure which quantify how well the reference image is aligned with the transformed template image. This measure is the quantitative criterion used for the Space Optimization procedure search defined by the parameters of the transformation.

Finally, Interpolation is used to evaluate the intensity of the points of the moving image in the off-grid points. In the light of this algorithmic schematization, it is immediately clear that co-registration is ultimately an optimization problem whose goal is to find the spatial mapping by which the template image is transformed until it is aligned with that fixed one.

2.2.1 Algorithms for Images Co-registration

One of the most used criteria for the classification of co-registration methods refers to the method in which the two input images are compared [9]. From this point of view, it is possible to identify four main categories of algorithms.

- **Manual co-registration**. In this context, the user (for example a radiologist) is requested to align images visually using image processing software tools
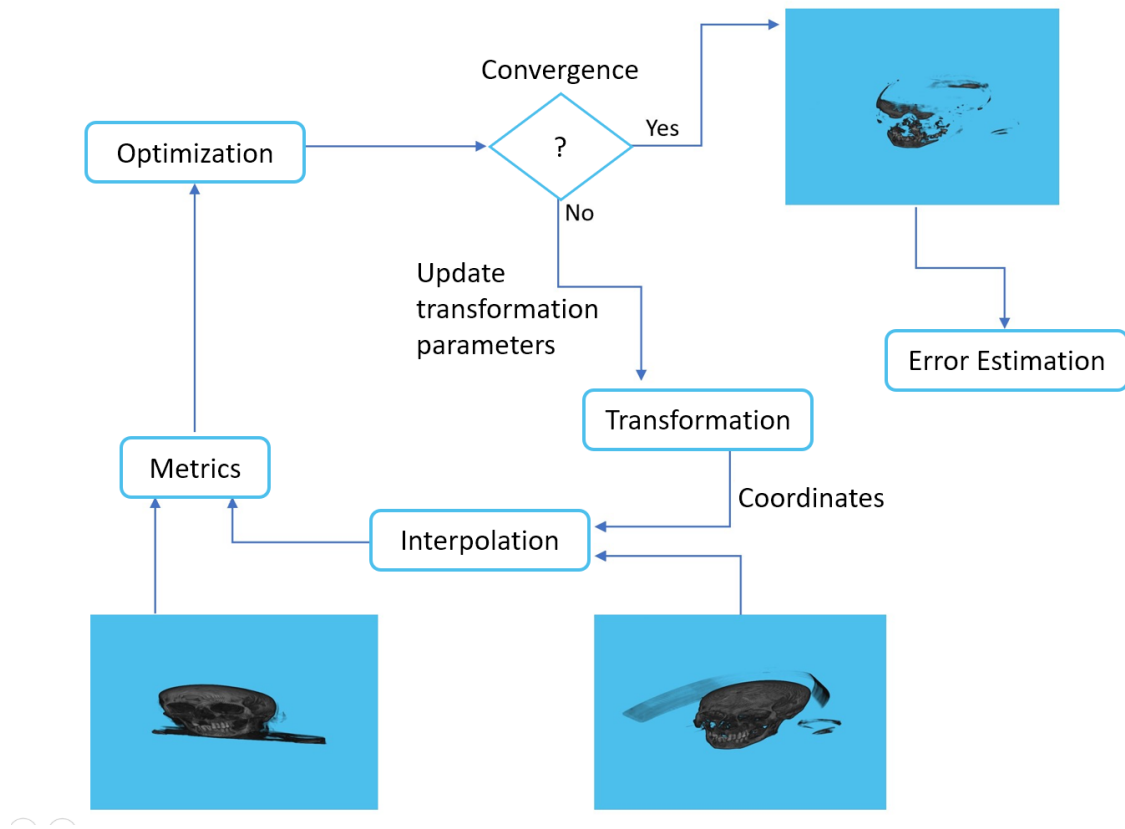
Figure 2.7. General Framework for Image Registration

with a particularly sophisticated graphic interface to the point of allowing easy data manipulation. Many medical applications (see e.g. [10]) provide the means for manual co-registration to align several types of images. This type of co-registration, however, has important limitations. Among these, the most important concerns accuracy, which depends on judgment and experience of the user as, in general, different users get different results.

- **Landmark-based co-registration**. Co-registration based on landmarks (i.e. markers fixed a priori) essentially consists in identifying the positions of points corresponding in the two images and in the subsequent determination of the transformation which aligns the pairs of these points. In the medical field, there are two types of markers: internal and external ones. The internal markers, known commonly as anatomical markers, they are detectable anatomical features and identifiable in the images. Their identification and cataloging is done by experts thanks to a software that allows the definition of the corresponding anatomical structures. The external markers, on the other hand, are objects attached to the patient during acquisition of the images, must be visible and easily identifiable objects. The procedure for carrying out a landmark-based co-registration essentially consists of of two steps:

  1. identification and coupling of the landmark (anatomical or external) in the reference images and template

2. calculation of the geometric transformation that minimizes the distance between the coordinates of landmark

Another more formal definition of landmark-based co-registration is the following: Given two sets of N corresponding points, P = p_i and Q = q_i (the points of the landmark pairs), we look for a transformation T that minimizes the square root of the spatial distance between corresponding points.

- **Surface-based Co-Registration**. Surface-based co-registration involves the extraction of surfaces of (anatomical) objects in images and the determination of transformations which minimize the distance between corresponding surfaces. Unlike landmark-based co-registration where markers are identified manually, surface-based techniques require the reconstruction of surfaces from a set of segmented contours in the various images. The success of these methods depends essentially from the segmentation stage. Besl and Mckay [11] presented a co-registration strategy general-purpose known as "Iterative Closest Point (ICP)". For each iteration of the process of co-registration, the closest point on a surface is determined by all the points relative to the corresponding surface. The correspondences of these points then are used to align the images optimizing the transformation.

- **Intensity-based co-registration**. Co-registration based on the intensity of the images/volumes is perhaps the most used in literature. From a statistical point of view, an image/volume can be seen as a distribution of a random variable (the intensity of the images). Intensity-based co-registration is based on the measure of similarity, or metric, of the images to be aligned and on the optimization of this measure, obtained changing the parameters of the transformation.

2.2.2 Measurement of Similarity and Metrics for Co-registration

As anticipated, the intensity-based co-registration method is the most widespread and is based on the assumption that it is possible to define a metric between images/volumes. For example in the two-dimensional case the metric must be understood as a generic quantitative measure that tells how well the *reference* and *template*(transformed) images are aligned. It can be based, for example, on the differences between the intensities of images (cross correlation, ssd), on statistical information (mutual information), on relationships in the space of image frequencies (phase correlation) or on other information. The selection of the type of metric to be use is highly dependent on the type of co-registration that it needs to be fixed. Some metrics have a broad capture spectrum, others require one initialization close to the optimal position. Some metrics are suitable for captured images with the same modality, others for different modalities. Ultimately, there is no well defined rule to decide which metric to use. The following are the most used and are the ones that turned out to be more versatile and efficient from the point of view of the results obtained.

Sum of Squares of Intensity Differences (SSD)

The SSD metric (acronym deriving from the English expression Sum of Squared Differences), is used for co-registrations of images that share the same modality (intra-modality). Examples of application of such metrics are: [12]. To estimate this metric, it is computed the average of the sum of the squares of the differences between intensity of corresponding pairs of points of the images to be co-registered. Give the pictures A and B the SSD value is defined as:

$$SSD(A, B) = \frac{1}{N} \sum_{i=1}^{N} \left(A_i - B_i^T \right)^2$$

where A_i is the i-th pixel of image A, B_i is the i-th pixel of image B, N is the number of pixels of the image A.

Cross-correlation coefficient (CC)

The cross-correlation coefficient, as the SSD metric, is used for intra-modality co-registrations. Given two images A and B the coefficient CC is given by the following expression:

$$CC(A, B) = -1 \times \frac{\sum_{i=1}^{N} \left(\left(A_i - \bar{A} \right) \cdot \left(B_i - \bar{B} \right)^T \right)}{\sqrt{\sum_{i=1}^{N} \left(A_i - \bar{A} \right)^2 \cdot \sum_{i=1}^{N} \left(B_i - \bar{B} \right)^2}}$$

where A_i is the i-th pixel of image A, B_i is the i-th pixel of image B, $\bar{A}$ and $\bar{B}$ are the mean values of the intensities of images A and B respectively, N is the number of pixels of the image A and T is the transformation.Some examples of applications using this metric could be found in [13].

Mutual Information

Mutual Information (MI) calculates the information in "common" between two images A and B. It measures the information that a random variable (an intensity of the image reference) carries with respect to another random variable (an intensity of the template image). The major advantage of using the MI is that there is no need to specify the form of dependence between variables and this makes MI suitable for multi-modal co-registration. Works and pubblications that led to the affirmation of the MI for the co-registration of images are: [14].
More formally, *mutual information* is defined in terms of entropy [15]. Let consider

$$H(A) = - \int p_A(a) \log p_A(a) da$$

the entropy of a random variable A, and H (B) the entropy of a random variable B and let

$$H(A, B) = - \int p_{AB}(a, b) \log p_{AB}(a, b) da db$$

the joint entropy of A and B.
If A and B are independent then

$$p_{AB}(a,b) = p_A(a)p_B(b)$$

and

$$H(A,B) = H(A) + H(B)$$

If between A and B there is a dependency it will be instead

$$H(A,B) < H(A) + H(B)$$

The difference

$$I(A,B) = H(A) + H(B) - H(A,B)$$

It is called *Mutual Information.*
If the reference and template imagese are alligned the MI reach its highest value.

2.2.3 Transformation Classes for Co-registration

A fundamental distinction between the different co-registration techniques is between techniques that make use of transformations based on rigid models (or rigid transformation) and those which, instead, are based on deformable models (or non-rigid transformation). The term non-rigid co-registration refers to a class of methods in which images have differences that cannot be modeled by similarity transformations (rotation, translation and scale transformation). The model, rigid or deformable, taken into consideration, however, takes into account the characteristics (physical or optical) inherent in the transformation that transforms one image onto another. A transformation can be stiff if it keeps the lengths and angles unchanged (isometry), not rigid if it causes deformations. Another distinction can be that of consider linear and non-linear transformations (nature of the transformation).
Transformation function models can also be divided into two broad categories depending on the amount of image data they use as their support. We'll have global models if the transformation function is applied to the whole image, we will have local models if the transformation will apply differently for different areas of the image (domain of transformation).
The choice of transformation for co-registration should be dictated by the presumed transformations or any deformations that exist between the images and that you want recover, from the types of images we are considering and the kind of accuracy that we seek.
Much of the initial work done in the field of medical image co-registration has concerned the co-registration of brain images of the same subject acquired according to different modalities (MRI, CT or PET) [16]. For these applications the use of a rigid transformation model is sufficient, given that the shape and position changes of the brain are negligible in the relatively short time between acquisitions. However,in many types of medical images, the type of deformation cannot be treated as rigid transformation.
In general this can happen in three different cases:

1. intra-patient registration but at different times with possible morphological changes in the part on which the analysis is performed;

2. inter-patient registration, due to the natural anatomical differences between different subjects;

3. registration aimed at correcting any artifacts and distortions.

Deformations of the first type occur, for example, in the case of variations due to growth (of anatomical parts, for example bones) or to surgical interventions, or to degenerative processes, such as in the case of diseases such as Alzheimer's, multiple sclerosis or malignant tumors [17]. In case of growth or degenerative processes, the changes are incremental and in the most of the cases can be represented by a differentiable transformation. In some conditions this may also be true in the case of changes due to surgical operations.

Type 2 deformations are encountered when comparing the anatomy of different people. For example, the neuro-anatomical differences between the brains of two different people are usually many, particularly in the cerebral cortex. To compare structural variations between individuals one can proceed by co-registering the images of each individual to an image atlas, in order to bring everything back to a single reference system to be used for the comparison [18].

Deformations of the third type are found, for example, in the case of resonance images magnetic (MR). For example, images acquired with EPI (Echo Planar Image) protocol, they can have severe geometric distortion. The distortion depends on the type of fabric, from the orientation of the subject with respect to the sensor and from the acquisition process itself of the MR image. Knowledge of the physics of the acquisition process can provide constraints to the estimate of the deformation. Clearly, the hypothesis that the optimal transformation is 'rigid' or 'affine' is very restrictive and in many cases it is not verified. Therefore, much of the recent work on the co-registration of medical images he was involved in the development of techniques non-rigid for applications ranging from correction of deformations of soft tissues, which may occur during the imaging process or an operation, to the modeling of the neuro-anatomy of the elderly and of the young [19].

Rigid transformation

The rigid body model includes only translations and rotations. Objects do not change shape, the distance between two points in the template image is preserved after the transformation that co-registers it to the reference image.
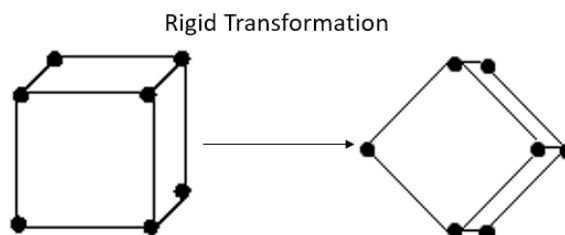

Figure 2.8. Rigid Transformation

Similarity

The similarity model [20]includes translation, rotation and scaling. The parallelism will be preserved if straight lines of the image reference will be mapped to straight lines in the template image.
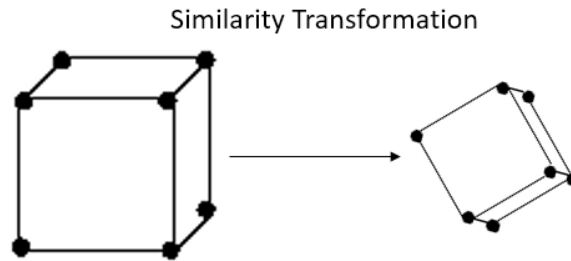

Figure 2.9. Similarity Transformation

Affine

Affine transformation consisting of translation, rotation, scale, and shear. Affine transformation, or an affinity (from the Latin, affinis, "connected with"), is a geometric transformation that preserves lines and parallelism but not necessarily distances and angles.
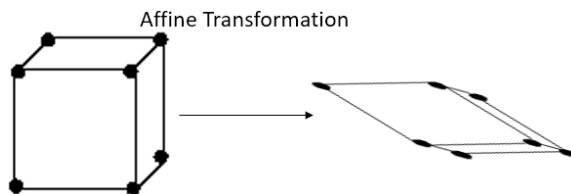
Figure 2.10. Affine Transformation

2.2.4 Optimization

Regardless of the type of representation chosen and the class of transformations used, the co-registration process basically consists in minimizing a cost function. After selecting the characteristics through which to represent the information content of the image, the choice of the cost function is substantially equivalent to defining a metric in the space of such characteristics. Furthermore, the choice of the cost function has some heavy repercussions on the type of minimization technique that can be used in the resolution of problem. For example, we often tend to define the cost function in such a way as to obtain a least squares problem, the solution of which, except for technical problems due to the number of the variables, is relatively simple and above all has a single global solution. Finding the maximum of the metric is a multidimensional optimization problem where the number of dimensions corresponds to the degrees of freedom of the expected geometric transformation. This task is entrusted to the optimizer whose choice therefore depends on the type of transformation used. More generally, if the cost function is sufficiently regular, there is a large number of standard

optimization techniques (see eg [21]). In the list below we list the methods in our opinion of more general applicability, with the reference to some of the works in which the method is applied to the problem of co-registration of images:

- Gradient Descent and its various modifications or adaptations to make it more efficient (used, for example, in [22]);

- Pseudo-Newton methods, in which the gradient components are rescaled with terms dependent on the Hessian matrix, such as the Levenberg-Marquardt gradient descent method;

- Stochastic gradient descent, where the gradient is estimated and not calculated exactly;

- Simulated annealing;

Chapter 3

Methods

The purpose of this thesis work is to provide new and more advanced supports to physicians specializing in Multiple Myeloma. Offering tools that base their operation on advanced algorithms is of fundamental importance for a more correct, faster and more refined final result.

At the moment there are no specific tools for the study of lesions caused by Multiple Myeloma so the following proposed methods were developed by me after analyzing the specific processes adopted today by doctors in order to assess their criticalities.

The main obstacle is the manual nature of most of the steps that make up the process. In fact, in order to evaluate the course of lesions caused by Myeloma, the doctor must manually extract the affected bone portions from two different CT scans and then check slice by slice the size and shape of the lesions in each of their sections to diagnose where there are differences and then make a volumetric estimate.

Another major obstacle to this process is the misalignment of the portions examined due to the position the patient assumes during CT scans. In fact it is not currently the practice to suggest the patient to maintain the same position every time he undergoes a CT scan and it may happen that sometimes the positions of portions such as the limbs or the direction of the head are in different positions.

This implies that even when the areas in which the same lesion is present are identified, this volume of interest is not split into the CT slices in the same way between the two temporal scans, and even if the lesions are identical their projections for each slice of the CT scan will be different and their comparison will be further compromised.

The methods developed were created and tested with data provided by the National Cancer Institute (INT), we were provided with 3 clinical cases, each containing CT scans performed one or two years later and in different resolutions.

Thanks to the use of these data it was possible to simulate real use cases, in fact the medical records containing the diagnoses and the description of the location of the lesions for each clinical case were provided, therefore it was possible to develop and verify the methods in optimal way.

This made it possible to optimize certain parameters such as the application of threshold values for the extraction of the bone component, or the optimization of the co-registration algorithm, based on data characteristics that comply with what will then be reported in real use cases.

The proposed methods replace the part of the work that the doctor must perform manually with advanced automatic algorithms, the Figure 3.1 shows the workflow for the study of the course of lesions caused by Multiple Myeloma with the proposed methods.
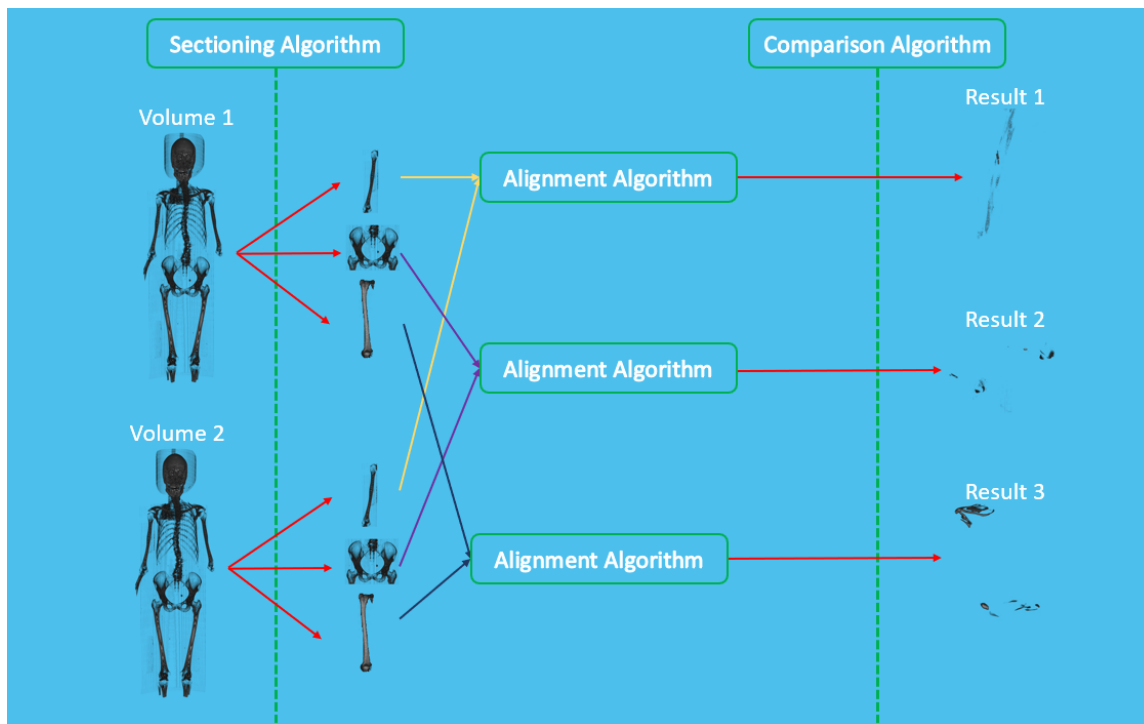

Figure 3.1. General workflow

The first step involves the definition and extraction of the volume portions to be analyzed, these sections can be areas already noted in a previous medical record if there is a patient history or, if it is a patient's first visit, can be areas containing bone portions definitely at high risk like flat bones.

This process is carried out by the **Sectioning Algorithm**, discussed in section 3.2 which is able to identify and extract the portions indicated by the doctor during the setup phase from total CT scans. Once the algorithm has been applied to a total volume of the patient's body, it will output subvolumes appropriately divided and isolated from the rest of the body to be analyzed individually.

This phase is of fundamental importance because it allows the isolation of the bone portions to be analyzed so that they can be aligned in the next phase.

To align the bone portions it is necessary to isolate the volumes because, again due to the position assumed by the patient during the acquisition phase of the CT scan, trying to align the entire body volume or large portions of it would be impossible.

This process is carried out by the **Alignment Algorithm** discussed in section 3.3 which, taking as input the same volume belonging to different total scans, therefore positioned differently in the space for example a forearm that in a first scan was along the hips in the second scan is above the chest, returns the two volumes in the same position in the 3D space. The algorithm does this by estimating the directions in which to move and rotate one of the two volumes to match the other.

Once the volumes have been extracted and aligned in a totally automatic way, it will be possible to calculate the difference, so as to highlight whether there are differences between the two portions, such as an increase in the volume of a lesion.

Thanks to this data it will be possible for the doctor to immediately identify the areas with the highest probability of having undergone changes so that he can subsequently make a more accurate visual comparison as well as a more precise study on the size and shape of the lesion. This could also be aimed at a further analysis in order to evaluate in time if a further course could compromise adjacent anatomical structures or the functionality of the same bone structure in which the lesion is located.

Both the Alignment and Sectioning algorithm are based on the **Co-Registration** process discussed in section 2.2, a robust and widely used image processing method. Furthermore, both algorithms implements a **Coarse-to-Fine** approach which refers to applying two consecutive methods to the same data, respectively to a low resolution and high resulting version of them. A method to a low-resolution version of the image as reported in Figure 3.2 with a resampling of 50% of the Total volume. In this case the volume's dimension before resampling was (512,512,534), after resampling it became (256,256,267).

All the computational processes can be applied to the low resolution volume and then the results can be applied to the high resolution volume after the conversion to the high resolution volumes coordinates.

The ability to choose the degree of resampling allows us to adapt the algorithms based on the type of volume to be studied, smaller volumes will not necessarily need resampling, larger volumes can be processed with resampling of different degrees based on the their extension.
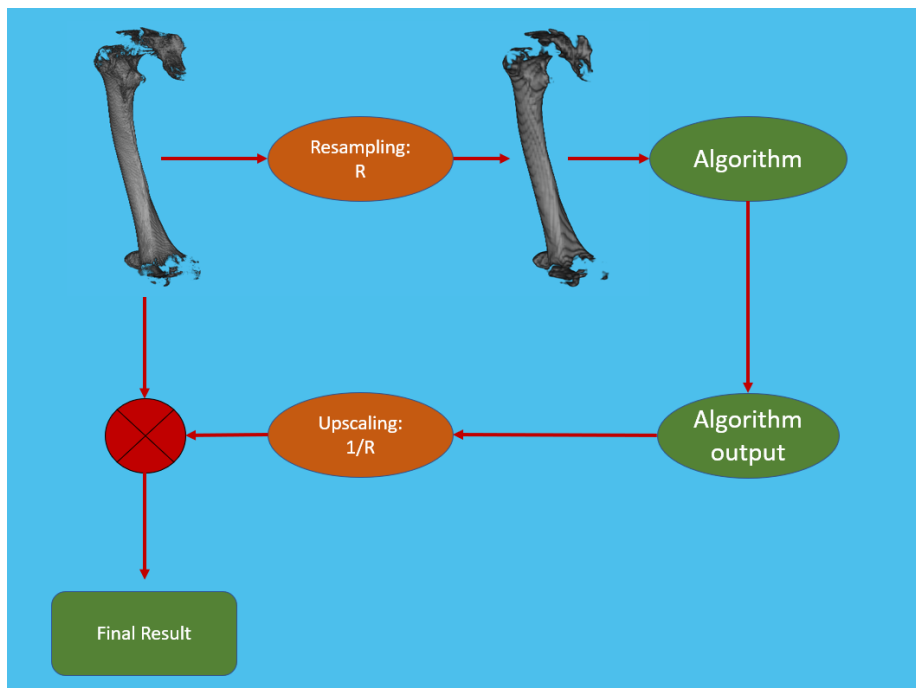

Figure 3.2. Resampling of a Bone Volume

The reduction of calculation times is fundamental for an application perspective because it allows an almost real-time calculation.

3.1 Data Analysis and Preprocessing

The preprocessing carried out on the data provided will be described in the next paragraph. This is a process of inspecting, cleansing, transforming, and modeling data with the goal of discovering useful information, informing conclusions, and supporting decision-making

The data provided to us are CT acquisitions in dicom format of different patients and on different dates. DICOM (Digital Imaging and COmmunications in Medicine) is a standard that defines the criteria for the communication, visualization, storage and printing of biomedical information such as radiological images. [23]

At first a data discovery process was carried out where 6 different acquisitions were examined, these acquisitions belong to 3 different patients with 2 acquisitions per patient made 12 or 24 months apart.

By doing this, it was possible to extract the most significant information from the metadata and carry out the drafting of the first Data Processing codes in order to work in Matlab environment on a file format generally used by specific software aimed only for the visual analysis. In particular, all the data provided to us, for each patient, contained multiple acquisitions with different characteristics and different points of view with respect to the patient's body.

These scans were acquired for an analysis aimed at studying Multiple Myeloma and the lesions caused by it with the methods described in the chapter 1.1.4. Therefore, the possibility of using imaging algorithms had not yet been evaluated and certain protocols that would have improved the obtainable results as well as extending the possibilities of the algorithms were not adopted.

An example of a protocol to be adopted is the choice of replicating the patient's position on the bed of the CT scan machine as closely as possible in the two time acquisitions. For example, the patient should be advised to keep his arms and legs always at his sides and his head facing the same direction. The radiologist on the other hand must try to place the patient in the same position with respect to the coordinates of the scan and carry out acquisitions for the same patient with the same step or the same resolution as those already present in the same patient's archive.

3.1.1 Data characteristics

A first approach was carried out with the managing of the data, these were provided to us without an appropriate directory as they were generated and stored with a proprietary method of the manufacturer of the machinery used for the acquisition of the scan.

Reorganizing the data is a step that has allowed us to speed up all subsequent phases and to proceed with data discovery.

From the metadata it was possible to trace the spatial characteristics of the scans, the dimensions of the voxels and other useful information for the development of the subsequent steps.

The individual dicom files have been analyzed and their metadata read, each dicom file belongs to a precise scan defined by the resolution (slice pitch) and by the portion of the body analyzed.

Finally, an algorithm was created that reorganized the data. In this step the raw

dicom files have been repositioned in subfolders, each of which contains all the files belonging to the same section. This part made it possible to load in the further steps the 3d volumes directly by selecting the specific volume to be processed, optimizing loading times.

Another important information was the compatibility between the different acquisitions for the same clinical case.

	SeriesDateTime	Rows	Columns	Frames	SeriesDescription	SeriesInstanceUID
1	24-Sep-2019 11...	512	512	1	Topogramma 0.6...	1.3.12.2.1107.5.1....
2	24-Sep-2019 11...	512	512	1	Topogramma 0.6...	1.3.12.2.1107.5.1....
3	24-Sep-2019 11...	0	0	1	Dose Report	1.3.12.2.1107.5.1....
4	24-Sep-2019 11...	512	512	1	Patient Protocol	1.3.12.2.1107.5.1....
5	24-Sep-2019 11...	512	512	408	testa-femore 3.0 ...	1.3.12.2.1107.5.1....
6	24-Sep-2019 11...	512	512	1528	testa-femore 1.0 ...	1.3.12.2.1107.5.1....
7	24-Sep-2019 17...	512	512	104	testa-femore 2.0 ...	1.3.12.2.1107.5.1....

Figure 3.3. 2019 data report of clinical case 1

	SeriesDateTime	Rows	Columns	Frames	SeriesDescription	SeriesInstanceUID
1		0	0	1	FUJI Basic Text ...	1.2.840.113845.11...
2	19-May-2020 09...	512	512	1	Topogramma 0.6...	1.3.12.2.1107.5.1....
3	19-May-2020 09...	512	512	2	Topogramma 0.6...	1.3.12.2.1107.5.1....
4	19-May-2020 09...	0	0	1	Dose Report	1.3.12.2.1107.5.1....
5	19-May-2020 09...	512	512	1	Patient Protocol	1.3.12.2.1107.5.1....
6	19-May-2020 09...	512	512	420	testa-femore 3.0 ...	1.3.12.2.1107.5.1....
7	19-May-2020 09...	512	512	1573	testa-femore 1.0 ...	1.3.12.2.1107.5.1....

Figure 3.4. 2020 data report of clinical case 1

In Figure 3.3 and Figure 3.4 it is shown the data characteristics summaries of the clinical case 1, acquired respectively in 2019 and 2020.

In the column named *Series Description* the name of the acquisition type is shown, the most important ones are the *testa-femore* followed by a number *3, 2* or *1*. The first part refers to the body part that are included in the volume scan so in this case the volume start from the head(testa) and finish to the femur(femore), the number instead refers to the size (in mm) of the space between the individual slices that make up the 3-D volume.

Consequently it is possible to see in the column *Frames* the number of slice composing the entire 3D Volumes while in the columns *Rows* and *Columns* the x and y dimension of each single slice.

Theese kind of informations allows us to proceed with our study with the knowledge that the voxel size (in mm) is the same for both the acquisitions of each patient, in fact, both cases shown in Fig.3.3 and Fig.3.4 contain the volumes *testa-femore 3.0* and *testa-femore 1.0*.

In other words we know that the spatiality of each slice is respected and further

comparison can be done, otherwise if their components weren't dimensionally equal we weren't allowed to compare the volumes unless they are brought to the same size by resampling.

With the aim of checking the size of the slices making up the volumetric acquisitions without spatial resampling, a check was carried out on each individual volume in different ways based on the type of information provided together with the data.

In some cases reading the specific field in the metadata was sufficient to check the correct voxel dimensions values, in other cases, perhaps due to different machine used to acquire the volume, this metadata field was absent so the Matlab tool *VolumeViewer3D* [24] was used.

VolumeViewer3D is a Matlab tool aimed to visualize, read and apply some calculations to 3d medical volumes in dicom format, for our case it was used for compute and show the voxel dimensions values.

For the usage of VolumeViewer3d a preprocessing on the data with the Dicom Manager Function Listing was mandatory, the function itself was not able to select and read the correct volumes between all the different Series present in the folder so the relocation of all the dicom file by SeriesDescription was needed.

In conclusion, it was verified that all three clinical cases provided to us contain at least one volumetric acquisition with equal spatial dimensions for both acquisition dates, in the following tables are reported all the data provided to us.

It will be specified the Clinical Case which to they belong and the names which we will refer to these volumes. Furthermore the acquisition year, the section name and the voxel size in mm is reported.

1. **Clinical Case 1**:

Volume Name	Year	Section	Size (mm)
Volume 1.1	**2018**	**Head-Knees 3.0**	**0.97x0.97x3**
Volume 1.1	2018	Head-Knees 1.5	0.97x0.97x1
Volume 1.2	**2020**	**Head-Femur 3.0**	**0.97x0.97x3**
Volume 1.2	2020	Head-Femur 1.0	0.97x0.97x0.8

Table 3.1. Clinical Case 1 Volumes data

2. **Clinical Case 2**:

Volume Name	Year	Section	Size (mm)
Volume 2.1	**2019**	**Bone**	**0.97x0.97x1.25**
Volume 2.1	2019	Bone	0.97x0.7x0.625
Volume 2.2	**2020**	**Bone**	**0.97x0.97x1.25**

Table 3.2. Clinical Case 2 Volumes data

3. **Clinical Case 3**:

Volume Name	Year	Section	Size (mm)
Volume 3.1	**2019**	**Head-Femur 3.0**	**0.97x0.97x3**
Volume 3.1	**2019**	**Head-Femur 1.0**	**0.97x0.97x0.8**
Volume 3.2	**2020**	**Head-Femur 3.0**	**0.97x0.97x3**
Volume 3.2	2020	Head-Femur 2.0	0.97x0.97x2
Volume 3.2	**2020**	**Head-Femur 1.0**	**0.97x0.97x0.8**

Table 3.3. Clinical Case 3 Volumes data

3.2   Sectioning Algorithm

This algorithm is able to automatically extract the skeleton portion of the volume supplied as input within a total volume, making the process of sectioning the volumes for the comparison of the individual parts automatic.

Isolating the portions of the body is the first step for the study proposed in this thesis work, the precision of this process is therefore essential for an accurate and precise comparison of parts of the patient's body acquired in different scans and it would be impracticable to propose a method in which the doctor selects each time the portion to be evaluated within the volume.
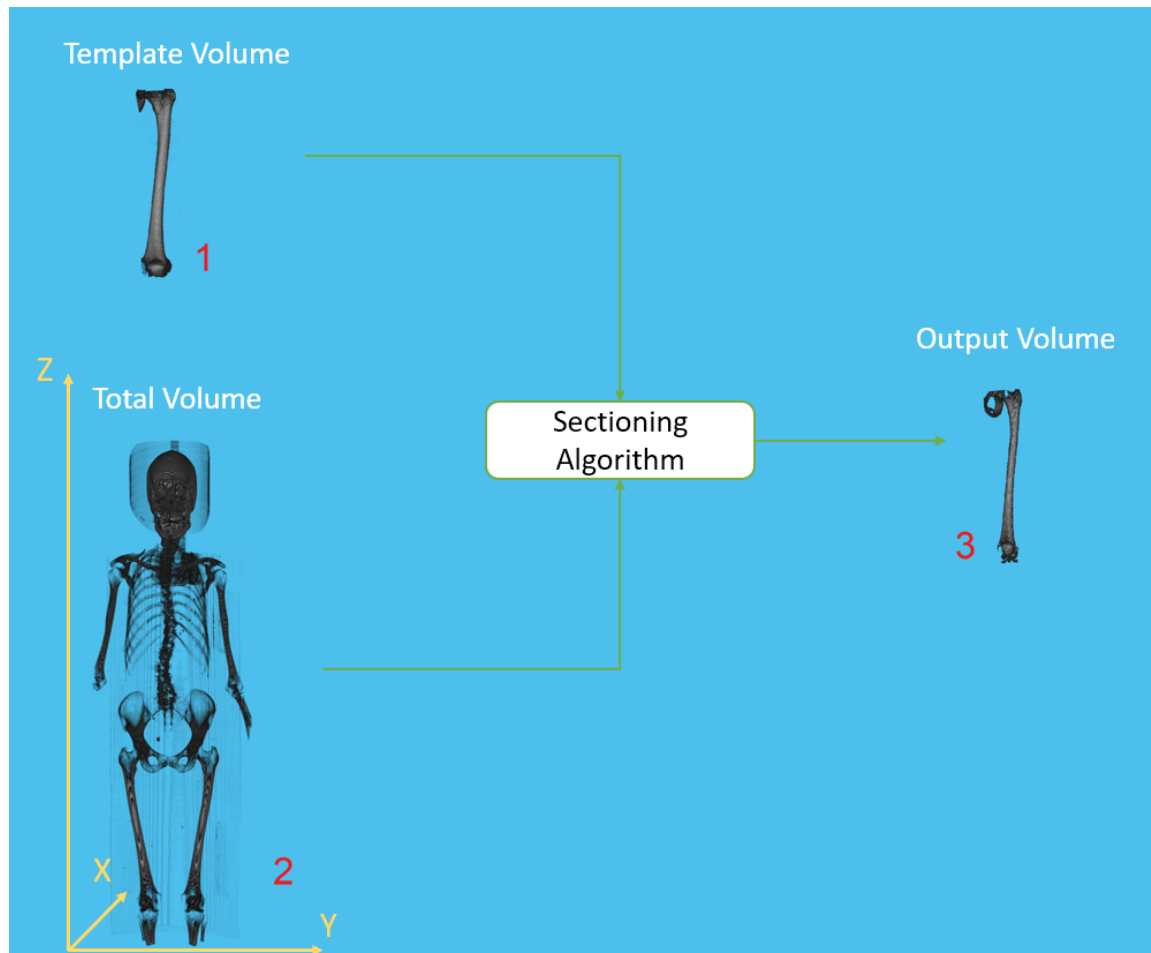

Figure 3.5. Results of the section algorithm applied to the femur.
1: *Template Volume*, 2: *Total Volume*, 3: *Algorithm Output Volume*

Automating the process of recognizing the parts of the body within the volume was therefore created to speed up and facilitate the doctor's work but can have other purposes.

In fact, the real big obstacle that did not allow us to implement deep learning algorithms is the absence of a proper labeled dataset for training a deep learning model. However, the creation of an appropriate dataset is a long process and, without the use of adequate tools, almost impossible to achieve. With the use of the sectioning algorithm it will therefore be possible, starting from total body scans, to build a

labeled dataset of body parts quickly and efficiently for future developments.

The algorithm is based on the volume registration function, a **Template Volume** is provided, which is the volume to search for, and a **Total Volume** in which to find the Template Volume, these two volumes belong to different reference systems which we refer to as spaces A and B.

The workflow, shown in Figure 3.7, can be divided in three big steps:

- **Pre-Processing** (Orange):

  1. The start and end point of the body in the z axis is calculated and divided into proportions.

  2. the Total volume is processed with respect to the area to be extracted, a cutout of the total volume is made based on the proportions of the adult human body shown in Figure 3.6, for example the head is 1/8 of the total body height or the legs are 1/2 of the total body height so extracting the corresponding part with a certain extent will include these portions.
     Once this process has been carried out, the portion of the body where we know the template volume is present is extracted. For example, in the case of the right femur, the right portion of the first half of the volume is extracted so the first 50% of the z-axis and the last 50% of the y-axis of the total volume is taken out.
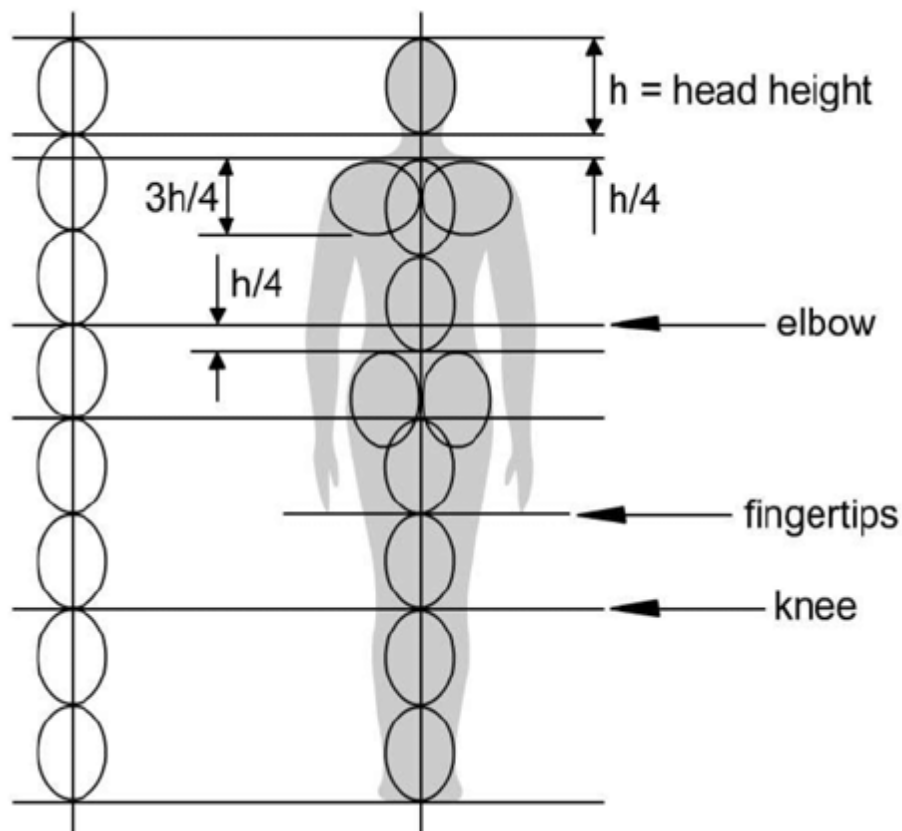

Figure 3.6. Human body proportion w.r.t. human head

- **Registration** (Green):

  1. The registration process is applied to the previously sectioned Total Body volume as *Fixed volume* and the Template Volume as *Moving Volume.*

  2. After the Template volume is aligned with the corresponding part the Rototranslation Matrix is computed, this is the matrix representing the instruction to align the Moving Volume with the Fixed volume.

  $$\begin{bmatrix} a_{11} & a_{12} & a_{13} & t_x \\ a_{21} & a_{22} & a_{23} & t_y \\ a_{31} & a_{32} & a_{33} & t_z \end{bmatrix}$$

  This Matrix is composed by the Rotation 3x3 matrix and the 3x1 Transversal Vector.

  3. The Rototranslation is applied to the Template Volume to align it, doing so the Volume will be moved in the Total Volume space coordinates.

  $$\begin{bmatrix} a_{11} & a_{12} & a_{13} & t_x \\ a_{21} & a_{22} & a_{23} & t_y \\ a_{31} & a_{32} & a_{33} & t_z \end{bmatrix} \begin{bmatrix} x \\ y \\ z \\ 1 \end{bmatrix} = \begin{bmatrix} a_{11} & a_{12} & a_{13} \\ a_{21} & a_{23} & a_{23} \\ a_{31} & a_{32} & a_{33} \end{bmatrix} \begin{bmatrix} x \\ y \\ z \end{bmatrix} + \begin{bmatrix} t_x \\ t_y \\ t_z \end{bmatrix}$$

  This means that a voxel previously belonging to the reference system *Space 1* is mapped in the reference system *Space 2* in the appropriate location generated after the application of the roto-translation matrix.

- **Coordinates Extraction** (Red):

  1. The coordinates of the Aligned Volume are retrieved and stored.

  2. The original Total Volume is sectioned in the coordinates extracted in the previous point, in doing so the final Volume is extracted containing the Total Volume portion we were looking for.

To further improve the method other steps are are carried out:

- **Course to Fine process**: In this case the registration process is applied to the entire TC volume, consisting of about 1500 slices in the case of the 1mm resolution. With this dimension it would take too long to iterate the process so the volumes were first re-sampled by scaling them by a value that range from 50% to 80% of the total resolution.
  Once the template volume location process is finished, and Coordinates of Final volume are computed it is applied an up-scaling to map the coordinates into the space of the original Total volume .
  Thus it is possible to obtain the Final volume in original resolution but facilitating the algorithm through the use of resampling.

- **Optimization of the registration**: as previously discussed in chapter 2.2.4: A fine tuning of co-registration parameters is carried out. These parameters have been suitably calibrated such as values that manage the number of maximum cycles, minimum value of the gradient and others. A fine tuning of these parameters was carried out for each specific case as different volumes portions have different sizes and a different number of slices as well as a different bone conformation that requires different settings to obtain an optimal result.

In Figure 3.7 it is possible to visualize each steps of the algorithm workflow described previously.
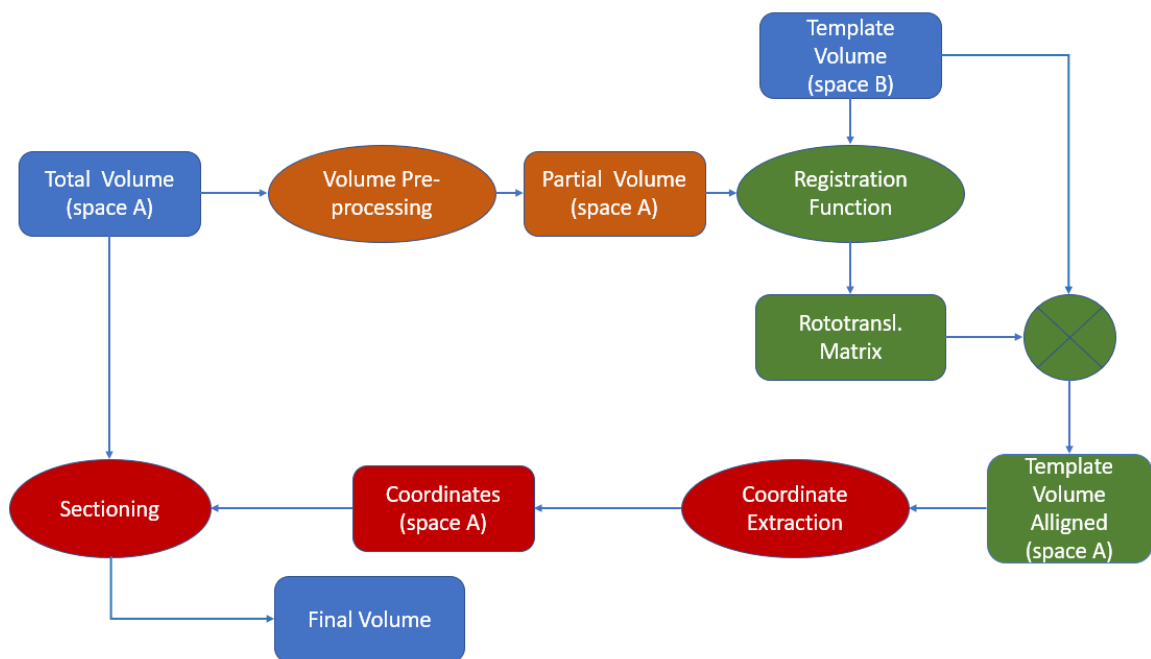

Figure 3.7. Workflow of the Sectioning Algorithm

Below is reported an example of the Matlab language implementation of the sectioning algorithm with motivated choice of the chosen parameters.

- Input Volumes are imported and the resampling value is set, this value can be chosen according to the size of the volume to be studied. If the volume is small it can also be equal to one to mean no resampling, if the volume is large these could cause a high computation time and a value as in the reported case of 0.5 can be chosen to mean a resampling of the 50 %.

```
—Setting input volumes—

res = 0.5;

fixed = Total_Volume;
moving = Template_Volume;

—Resampling for Coarse−to−Fine approach—
```

```
moving_rs = imresize3(moving, R);
fixed_rs = imresize3(fixed, R);
```

- The parameters of the co-registration function have been optimized with a maximum number of 500 cycles and an initial radius value equal to 1/10 of the standard one.
  These parameters can be chosen to refine the recording process, a higher number of cycles and a lower Initial Radius represent a finer and more accurate recording process at the expense of computation time.

```
——Registration Optimization——

[optimizer, metric] = imregconfig('monomodal');
optimizer.MaximumIterations = 500;
optimizer.InitialRadius = optimizer.InitialRadius/10;
```

- Then the Registration function is applied to the resampled volumes and the rototranslation matrix is computed.

```
——Apply co-registration function——

tform = imregtform(moving_rs, fixed_rs, 'rigid',
optimizer, metric, 'DisplayOptimization',1);
tform.T;
```

- The rototranslation matrix is applied to the moving volume which is aligned and moved to the Total Volume coordinates space.

```
——Align moving volume——

Rout = affineOutputView(size(fixed_rs),tform,
'BoundsStyle', 'SameAsInput');
moving_reg = imwarp(moving_rs, tform, 'bilinear',
'outputView', Rout);
```

- The coordinates of the aligned volume are extracted and reported to the original resolution. This process is carried out by calculating the minimum and maximum values of the coordinates of the non-zero voxels in the three dimensions.

```
——Compute Final Coordinates——
upscale = 1/res
ind= find(moving_reg);
[i,j,k] = ind2sub(size(moving_reg), ind);
min_i = (min(i))*upscale;
max_i = (max(i))*upscale;
min_j = (min(j))*upscale;
max_j = (max(j))*upscale;
min_k = (min(k))*upscale;
max_k = (max(k))*upscale;
```

- The Final volume is extracted by sectioning the Total Volume with the coordinates computed before.

  —Extract Final Volume—

  $$\text{final\_volume} = \text{Total\_volume}(\text{min\_i:max\_i},$$
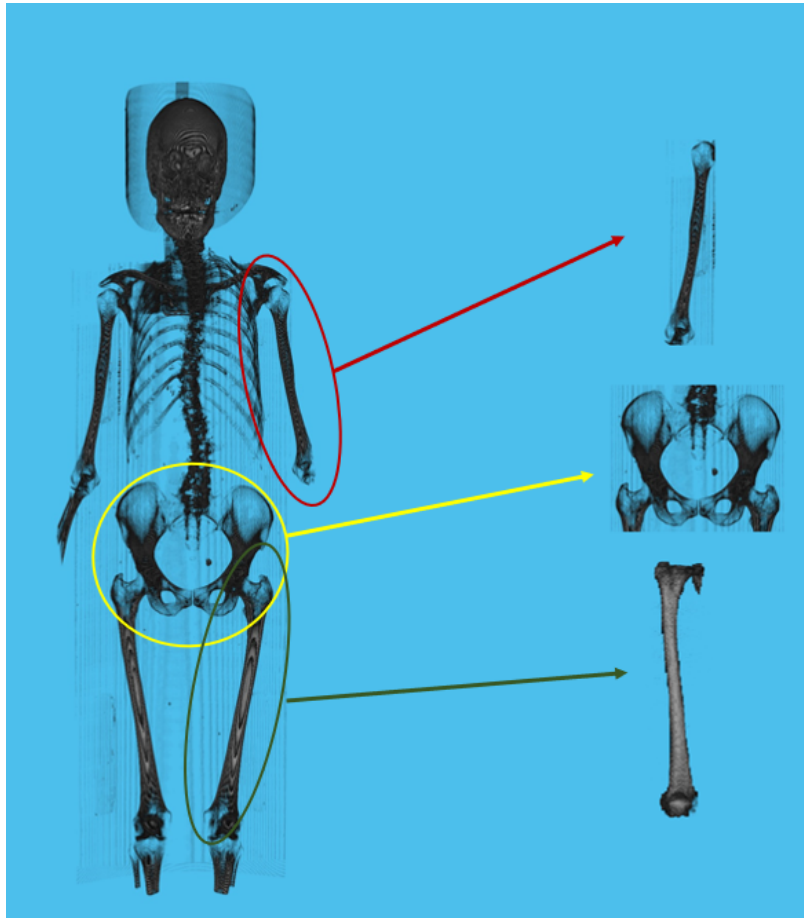 $$\text{min\_j:max\_j},$$
  $$\text{min\_k:max\_k});$$

Figure 3.8. Volumes sectioned with the Sectioning Algorithm from a Total volume

3.3 Alignment Algorithm

As anticipated, the main object of this thesis work is to provide support to the doctor in the search for changes in bone lesions due to Multiple Myeloma. The basic concept is to compare two CT scans and evaluate the bone components finding differences between them, especially in the areas where Multiple Myeloma lesions has been identified in a first diagnosis made by the doctor.

In order to compare two volumetric regions it is necessary to align them as applying the difference between non-aligned volumes produces an incorrect and uninterpretable result. The misalignment between these volumes is caused by the position that the patient assumes during the CT scans which cannot be perfectly replicated especially when scans are acquired one or more years apart. The components that contribute to the misalignment are two:

- the position that the patient assumes with respect to the space of the CT scan, for example the position along the z axis

- how the patient places himself on the bed, for example the arms are sometimes brought back to the sides and sometimes on the chest or the head turned slightly up or down.
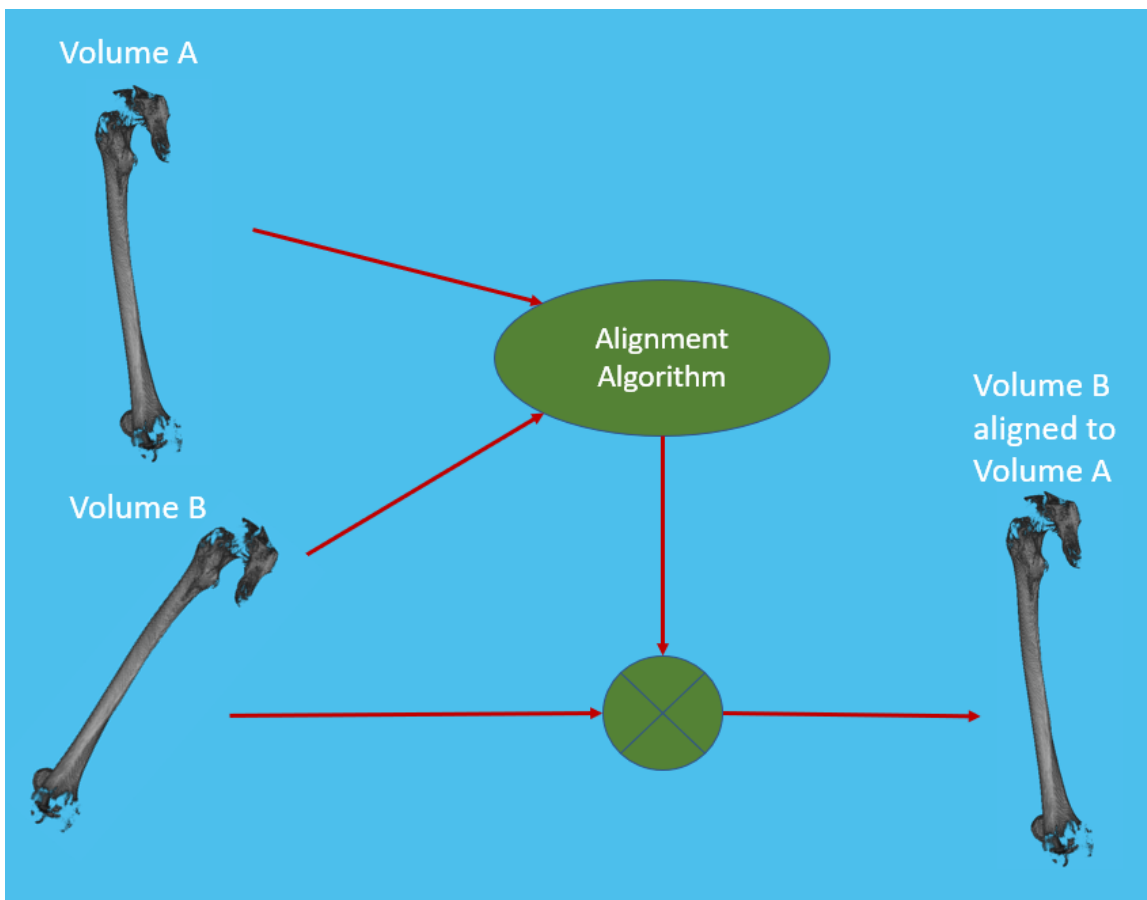

Figure 3.9. Example of the Alignment Algorithm application

The algorithm is based on the volume registration function, in this case the volumes supplied as input to the registration algorithm are two bone volumes extracted from different total volumes with the Sectioning algorithm discussed previously, we will refer to these two bone volumes as **Sections** 1 and 2. The general algorithm workflow, described in Figure 3.12 can be divided into three big steps:

- **Pre-Processing**(Orange):

  1. The two CT scans to be compared are selected;
  2. Once the portion to be compared is known, a volume template of the portion is used and through the use of the sectioning algorithm the Sections to be compared are extracted from the two total volumes;
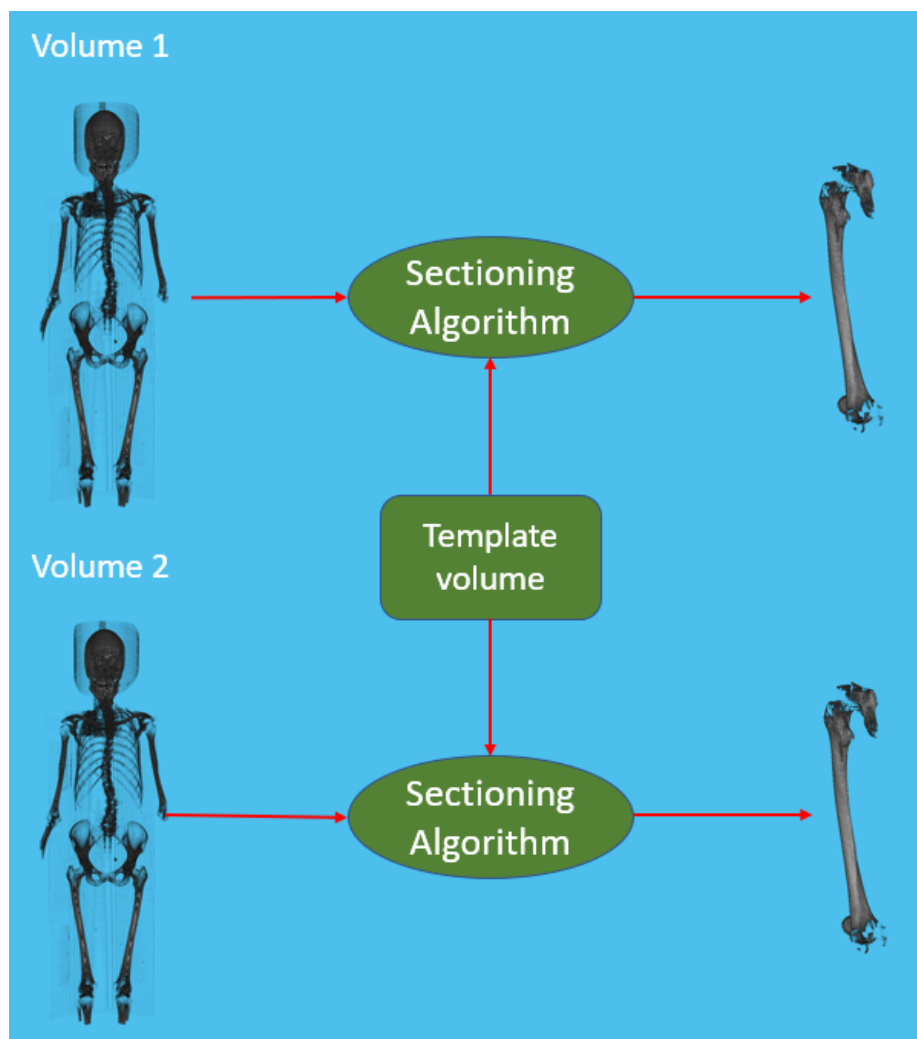

Figure 3.10. Caption

- **Registration** (Green):

  1. The two sections are supplied to the recording algorithm, one as Moving Volume and the other as Fixed Volume, the first will be the volume that the algorithm will "move" in order to be aligned with the corresponding part of the Fixed Volume.
     Once the alignment is done, the Roto-Translation matrix is produced, this is the matrix that represents the instructions for aligning the two volumes of the sections.

     $$\begin{bmatrix} a_{11} & a_{12} & a_{13} & t_x \\ a_{21} & a_{22} & a_{23} & t_y \\ a_{31} & a_{32} & a_{33} & t_z \end{bmatrix}$$

  2. The roto-translation matrix is applied to the Section Volume previously used as Moving Volume so as to align it with the other Section Volume and the Aligned Section Volume is produced.

     $$\begin{bmatrix} a_{11} & a_{12} & a_{13} & t_x \\ a_{21} & a_{22} & a_{23} & t_y \\ a_{31} & a_{32} & a_{33} & t_z \end{bmatrix} \begin{bmatrix} x \\ y \\ z \\ 1 \end{bmatrix} = \begin{bmatrix} a_{11} & a_{12} & a_{13} \\ a_{21} & a_{23} & a_{23} \\ a_{31} & a_{32} & a_{33} \end{bmatrix} \begin{bmatrix} x \\ y \\ z \end{bmatrix} + \begin{bmatrix} t_x \\ t_y \\ t_z \end{bmatrix}$$

- **Difference Computation** (Red):

  1. The difference between the aligned Section Volumes is calculated and the representative volume produced.
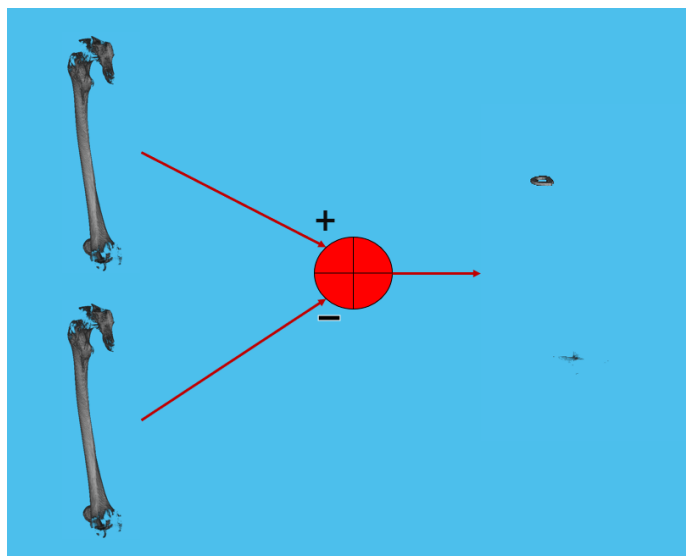

Figure 3.11. Difference between aligned volumes

With this type of data the differences between the two volumes will be enhanced and these portions will be labeled as having higher priority. These could be more likely to represent changes in lesions caused by myeloma, it is up to the doctor to analyze the points individually and diagnose their nature.

2. The spatial dimension of the volume is calculated, using the metadata related to the ct scans it is possible to calculate the size in mm of the identified portions. This is also very useful for the doctor to evaluate a future course and future compromises of the bone system.

To further improve the method other steps are are carried out:

- **Course to Fine process**: In this case, in the preprocessing phase, to optimize the process of extracting the portion from the total volume, a resampling of the volumes is carried out. In fact if the registration process is applied to the entire TC volume, this volume consist of about 1500 slices in the case of the 1mm resolution. With this dimension it would take too long to iterate the process so the volumes were first re-sampled by scaling them by a value that range from 50% to 80% of the total resolution.
  Once the template volume location process is finished, and Coordinates of Final volume are computed it is applied an up-scaling to map the coordinates into the space of the original Total volume.
  Thus it is possible to obtain the Final volume in original resolution but facilitating the algorithm through the use of resampling.

- **Optimization of the Registration**: as previously discussed in chapter 2.2.4: A fine tuning of co-registration parameters is carried out. These parameters have been suitably calibrated such as values that manage the number of maximum cycles, minimum value of the gradient and others. A fine tuning of these parameters was carried out for each specific case as different volumes portions have different sizes and a different number of slices as well as a different bone conformation that requires different settings to obtain an optimal result.
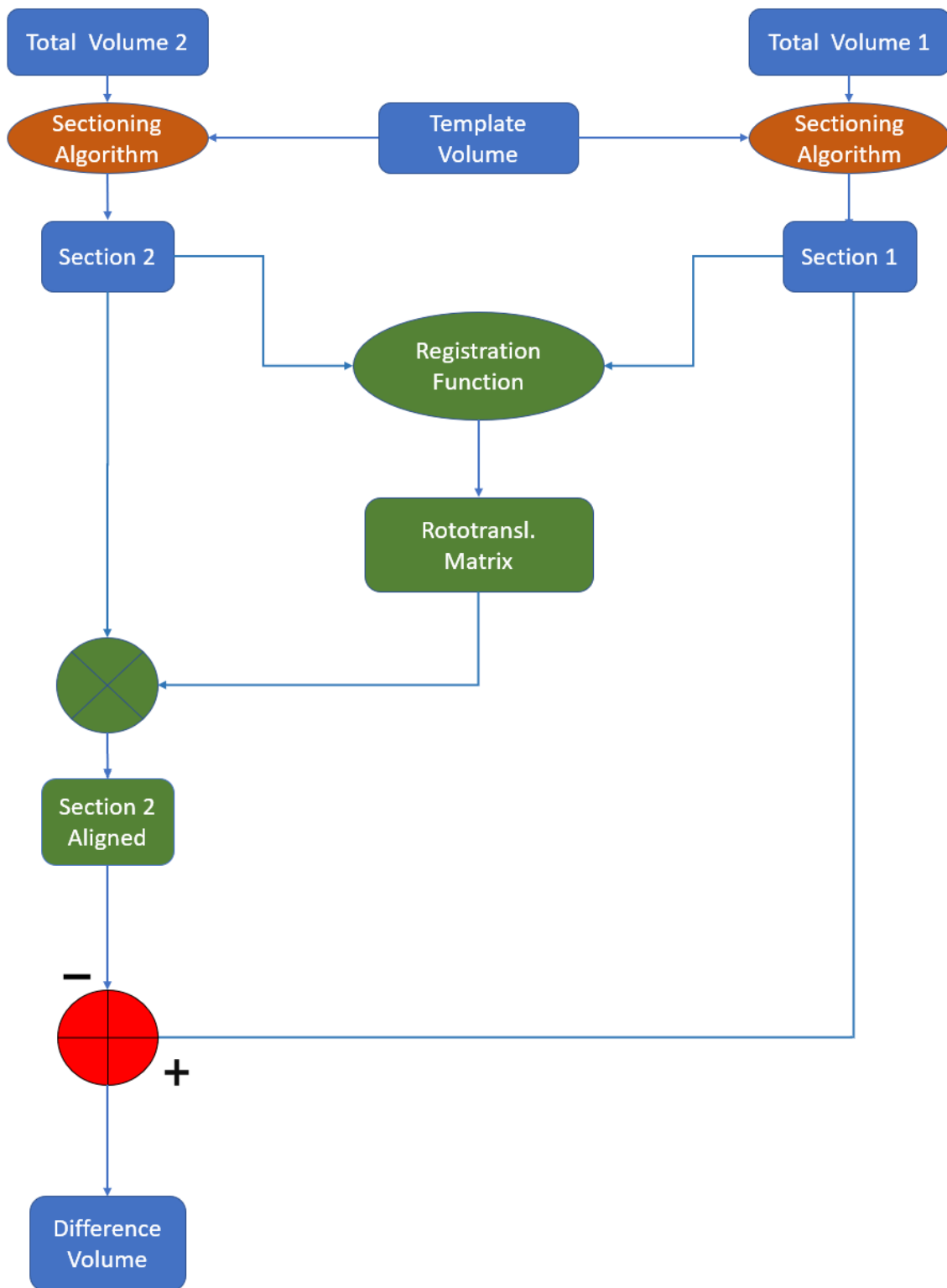
Figure 3.12. Workflow of the Aligning Algorithm, blue squares are the Volumes or subvolumes, orange ovals are the Preprocessing step, green part are the Registration step and the red part is the final Difference Computation

Below is reported an example of the Matlab language implementation of the sectioning algorithm with motivated choice of the chosen parameters.

- For the Pre Processing step:

1. the two Total Volumes are both thresholded and resampled by chosen values, in this case 0.8 as threshold and 0.5 as resampling. This is done to respectively optimize the registration function by filtering only the bone portion of the volume and exploit the coarse to fine process by reducing the overhall dimension of the volume.

```
——Setting input volumes——

res = 0.5;
threshold = 0.8;
fixed_1 = Total_Volume_1;
fixed_2 = Total_Volume_2;
moving = Template_Volume;

fixed_1(fixed_1<threshold)=0;
fixed_2(fixed_2<threshold)=0;
moving(moving<threshold)=0;

moving_rs = imresize3(moving, res);
fixed_1_rs = imresize3(fixed_1, res);
fixed_2_rs = imresize3(fixed_2, res);
```

2. The parameters of the co-registration function have been optimized with amaximum number of 500 cycles and an initial radius value equal to 1/10 of thestandard one.These parameters can be chosen to refine the recording process, a higher numberof cycles and a lower Initial Radius represent a finer and more accurate recordingprocess at the expense of computation time.

```
——Registration Optimization——

[optimizer, metric] = imregconfig('monomodal');
optimizer.MaximumIterations = 500;
optimizer.InitialRadius = optimizer.InitialRadius/10;
```

3. Then the Registration function is applied to the resampled volumes and the rototranslation matrix is computed.

```
——Apply co−registration function——

tform_1 = imregtform(moving_rs, fixed_1_rs, 'rigid',
optimizer, metric, 'DisplayOptimization',1);

tform_2 = imregtform(moving_rs, fixed_2_rs, 'rigid',
optimizer, metric, 'DisplayOptimization',1);
```

4. The rototranslation matrix is applied to the moving volumes which are aligned and moved to the Template Volume coordinates space.

```
——Align moving volumes——

Rout_1 = affineOutputView(size(fixed_1_rs),tform_1,
'BoundsStyle', 'SameAsInput');
moving_reg_1 = imwarp(moving_rs, tform, 'bilinear',
'outputView', Rout);

Rout_2 = affineOutputView(size(fixed_2_rs),tform_2,
'BoundsStyle', 'SameAsInput');
moving_reg_2 = imwarp(moving_rs, tform, 'bilinear',
'outputView', Rout);
```

5. The coordinates of the aligned volume are extracted and reported to the original resolution, then volume is extracted by sectioning the Total Volume with the coordinates computed.

```
——Compute Final Coordinates——

upscale = 1/res;
ind_1= find(moving_reg_1);
[i,j,k] = ind2sub(size(moving_reg_1), ind_1);
min_i_1 = (min(i))*upscale;
max_i_1 = (max(i))*upscale;
min_j_1 = (min(j))*upscale;
max_j_1 = (max(j))*upscale;
min_k_1 = (min(k))*upscale;
max_k_1 = (max(k))*upscale;

ind_2= find(moving_reg_2);
[i,j,k] = ind2sub(size(moving_reg_2), ind_1);
min_i_2 = (min(i))*upscale;
max_i_2 = (max(i))*upscale;
min_j_2 = (min(j))*upscale;
max_j_2 = (max(j))*upscale;
min_k_2 = (min(k))*upscale;
max_k_2 = (max(k))*upscale;

——Extract final Section——

Section_1 = Total_volume(min_i_1:max_i_1,
                         min_j_1:max_j_1,
                         min_k_1:max_k_1);

Section_2 = Total_volume(min_i_2:max_i_2,
                         min_j_2:max_j_2,
```

$$\text{min\_k\_2:max\_k\_2);}$$

- for the Registration step:

  1. The Registration function is applied to the resampled volumes and the rototranslation matrix is computed.

     ```
     ——Apply co−registration function——

     fixed = Section_1;
     moving = Section_2;

     tform_1 = imregtform(moving, fixed, 'rigid',
     optimizer, metric, 'DisplayOptimization',1);
     tform.T;
     ```

  2. The roto-translation matrix is applied to the Section Volume previously used as Moving Volume so as to align it with the other Section Volume.

     ```
     moving_reg = imwarp(moving, tform, 'bilinear',
     'outputView', Rout);
     ```

- for the Difference Computation the difference of the volumes is computed and plotted.

     ```
     diff = fixed−moving_reg;
     volumeViewer(abs(diff));
     ```

Finally, a visual demonstration of the importance of using the alignment algorithm is reported. Below is a visual example of the difference between two volumes with and without using the alignment algorithm.

The Figure 3.13 shows the two volumes "*Section 1*" and "*Section 2*" with the application of a threshold to extract the bone component.
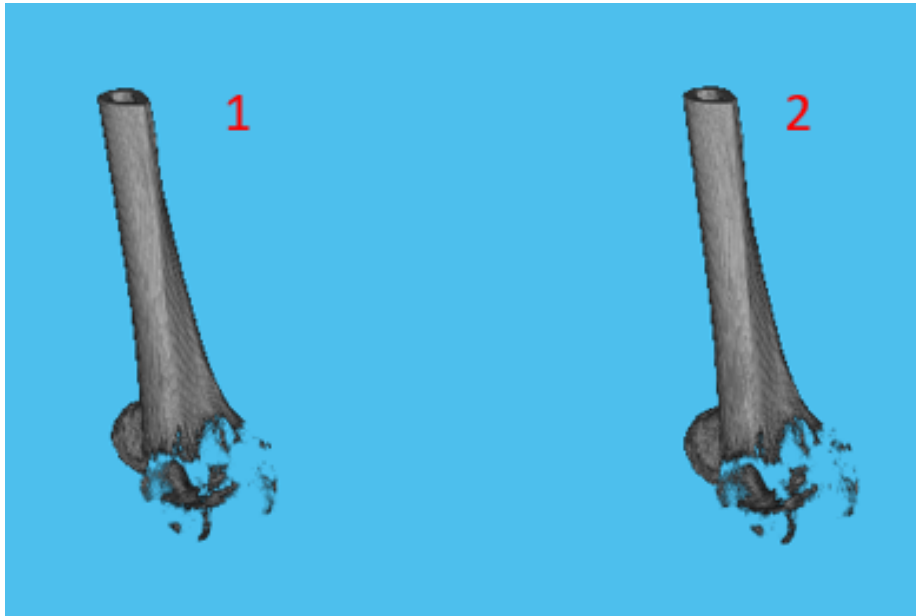

Figure 3.13. Section 1 and Section 2 with a tresholding applied to extract the bone portion

In Figure 3.14 are shown visual results of the difference of the two Sections volumes with and without the application of the Aligning Algorithm.
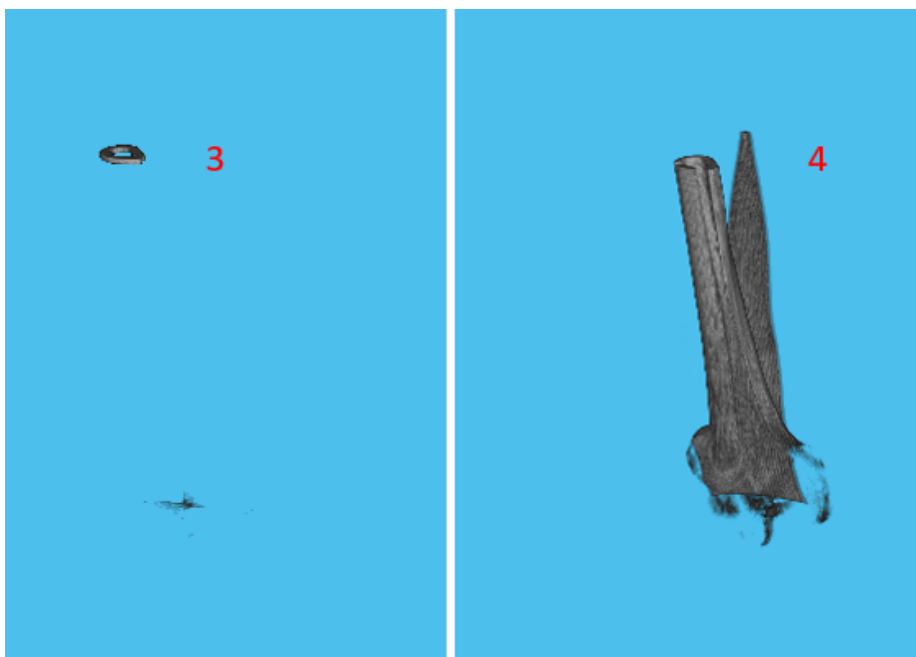

Figure 3.14. Difference Results with and without the application of the Aligning Algorithm

The importance of applying the alignment algorithm is shown, in the case in which the algorithm is correctly applied (section 3 of the Figure 3.14) are shown indicative data of the differences between the two sections, in this case a top area of the femur resulting due to a not perfect replication of the result obtained by the sectioning algorithm on the two total volumes.

In fact, one section includes this bone portion more than the other and this is correctly shown in the volume of the difference, confirming a correct result of the alignment algorithm.

If the alignment algorithm is not applied before making the difference between the two sections, the result obtained is a result that cannot be interpreted as shown in section 4 of the Figure 3.14.

Chapter 4

Results

In this chapter the effectiveness of the proposed method described in Chapter 3 will be demonstrated and the most important results obtained through the use of the developed methods will be shown.

For the Sectioning Algorithm what we want to demonstrate is the effectiveness of the algorithm, the possibility of using generic volumes as template volumes not belonging to the patient himself and the development of methods aimed at improving the results obtainable by the algorithm such as the application of a controlled extension of the sectioned volume.

This result therefore allows the implementation of this algorithm not only in a first diagnosis of a new patient who therefore does not have an archived scan history but also in the use for the creation of a specific dataset containing labeled bone volumes that can be used for the application of advanced deep learning algorithms in future developments.

The results were collected with the application of the algorithm with the data provided by the National Cancer Institute (INT), these are real clinical cases so the results collected represent the real possibilities that these methods can offer in real world operations.

For the Alignment Algorithm what we want to demonstrate is the precision of the algorithm, the ability to identify even the smallest differences between the same lesion that has had a course over time.

The results obtained with different optimization processes such as the application of a threshold or the resampling of the volumes supplied as input to the algorithm will also be shown.

Also in this case the data used to test the method are real clinical cases and also in this case the results collected are representative of the possibilities that this method would have in real use cases.

Finally, two clinical cases examined will be shown, to which the whole workflow will be applied starting from the Sectioning Algorithm up to the qualitative and quantitative assessment of lesions courses.

4.1 Sectioning Algorithm Results

In this chapter the results related to the Sectioning Algorithm will be discussed and reported, the purpose of this algorithm is to extract an Output Volume using two volumes, the Total Volume and the Reference Volume.

- **Output Volume**: volume of the skeleton section we want to extract;

- **Reference Volume**: volume used to guide the algorithm in the search, this volume must be a bone portion similar to the one we want to extract, when previous CT scans of the same patient are available it is possible to extract the reference volume from there;

- **Total Volume**: general volume from which to extract the sections, for example a new CT scan acquired;

The performance of the algorithm was evaluated with the process shown in Figure 4.1 and explained below:
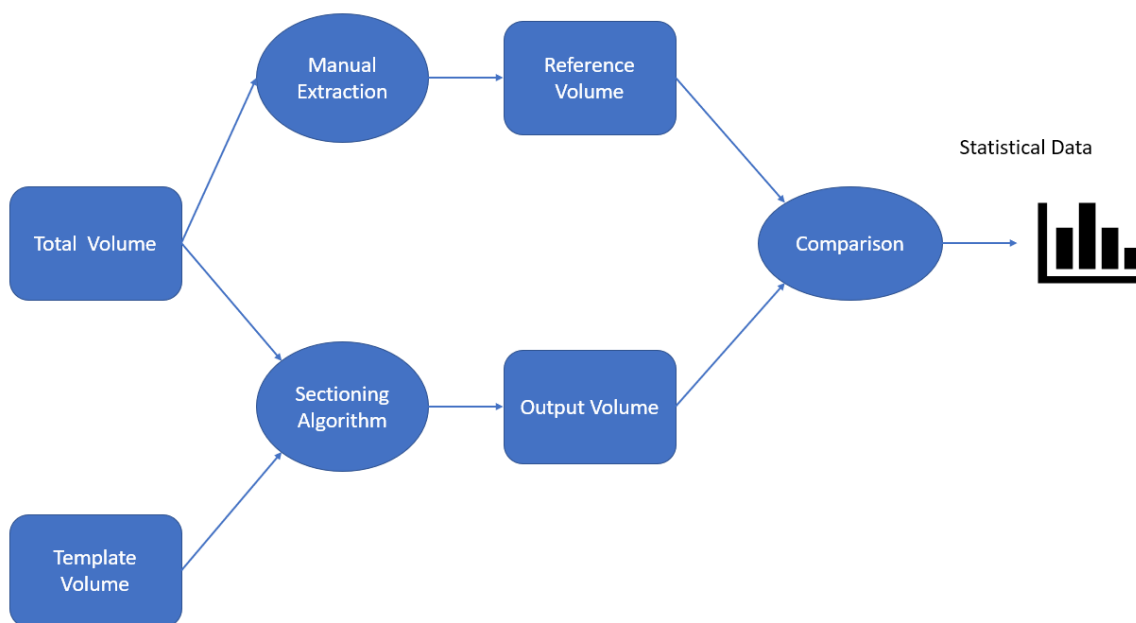

Figure 4.1. workflow for evaluating the accuracy of the Sectioning Algorithm

1. **Extraction of the bone portion of the Reference volume**:
   The *Reference Volume* is manually extracted by an operator from the available Volume which can be a previous scan of the same patient or a generic scan. Then a threshold is applied so as to extract only the bone portion.
   Once the exclusive presence of the bone portion of the reference volume ensured, a label "**Reference Voxels**" is applied to the voxels;

2. **Applying the Algorithm and Extracting the Output Volume**:
   the *Sectioning Algorithm* is applied to the *Total Volume* to let the Algorithm automatically find the *Reference Volume* as done manually in point 1, in this case the volume found by the algorithm will be the *Output Volume*.
   This work is carried out using a *Template Volume* to drive the algorithm.

3. **Extraction of the bone portion**:
   Once the *Output Volume* has been generated, the **bone portion** is extracted by applying a threshold. After checking the presence of the bone portion only, excluding all soft tissues, an "**Output Voxels**" label is assigned to the volume voxels.

4. **Statistical Data extraction**:
   With the collected data and the appropriately classified voxels it is possible to calculate the number of voxels of the following categories:

   - True Positives (TP): Voxels correctly belonging to the Output Volume as they are part of the desired bone portion.
   - False Positives (FP): Voxels mistakenly belonging to the Output Volume as they belong to different bone portions than the desired one.
   - True Negatives (TN): Voxels correctly excluded from the Output Volume as they do not belong to the desired bone portion.
   - False Negatives (FN): Voxels erroneously excluded from the Output Volume as they belong to the searched bone portion.
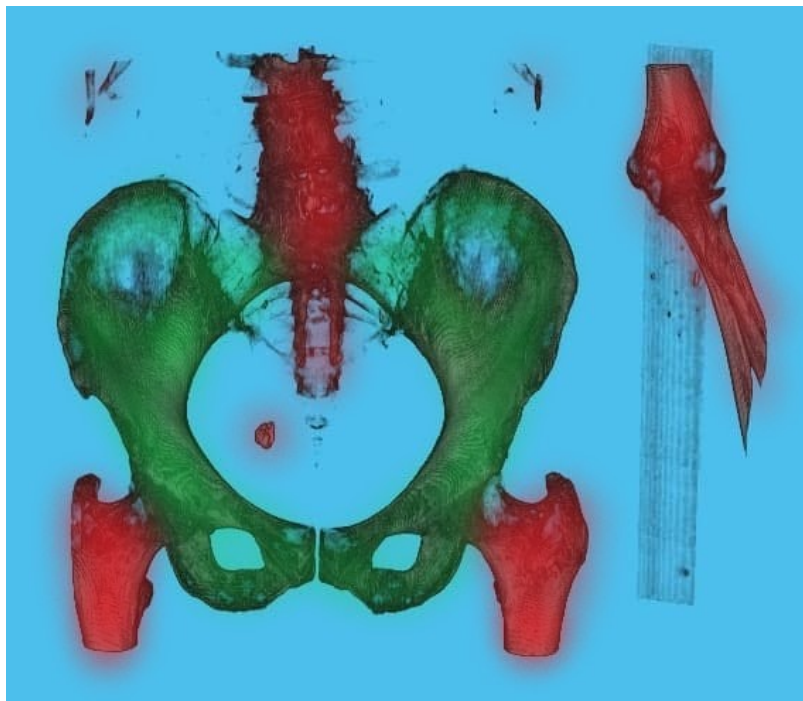

Figure 4.2. Example of voxel Labeling in the sectioning of the hip bone, the red-tinted voxel are labeled as False Positive while the green-tinted voxel are labeled as True Positive

5. **Calculation of statistical descriptors**:
   Once the statistical data have been collected to describe the results obtained by the algorithm, the following measures are calculated:

   - **Sensitivity** (True Positive rate) measures the proportion of positives that are correctly identified (i.e. the proportion between the Reference Voxels and the totality of the Voxels of the Output volume).

$$Sensitivity = \frac{TP}{TP + FN}$$

   It represents the algorithm's ability to identify the correct portions.

   - **Specificity** (True Negative rate) measures the proportion of negatives that are correctly identified (i.e. the proportion of the number of voxels belonging to the total volume and not contained in the output volume and the totality of the voxels of the total volume).

$$Specificity = \frac{TN}{TN + FP}$$

   It represents the algorithm's ability to exclude incorrect portions.

The following table shows the most significant results obtained from the application of the Sectioning Algorithm on different parts of the body in different clinical cases. Furthermore, two types of volumes were used as Template Volume:

- A volume belonging to the same clinical case.

- A volume belonging to another clinical case.

Clinical Case	Section	Template Volume	Sensitivity	Specificity
1	Femur	Other Patient Template	71%	78%
1	**Femur**	**Same Patient Template**	**85%**	**92%**
2	Hip	Other Patient Template	76%	82%
2	**Hip**	**Same Patient Template**	**96%**	**98%**
2	Femur	Other Patient Template	85%	88%
2	**Femur**	**Same Patient Template**	**96%**	**97%**

Table 4.1. Sectioning Algorithm Results

It is immediate to notice how the use of a volume belonging to the same patient as Template Volume produces better results, in any case, using generic template volumes or from other patients, good results have been obtained.
These results can be further improved with the application of an extension of the Output Volume coordinates as is shown in Figure 4.3. The value of expansion of the volumes can be easily tuned for each specific case and in which dimension, in fact, after the sectioning has been carried out, the doctor can easily evaluate whether the desired portion is included in the output volume, if this is not the case then he can

act by applying an extension in one, on two or on all 3 available dimensions so as to produce an optimal result.

This process improve the Sensitivity value up to results close to 100%, managing to include all the bone volume sought.

On the other hand, the application of this expansion process cause a decrease in the Specificity value as with the extension of the volume also unwanted bone portions are included, however this result is acceptable as the main purpose is to find and select the searched bone portion in its entirety, which can be a difficult process to achieve specially in volumes sections composed of multiple moving part such as the cranium with the jaw or the hip bone with the femur joints.

These sections are particularly problematic due to their structure, in fact they are composed of several parts with the possibility of moving between them and this characteristic is the cause of a less precise result.
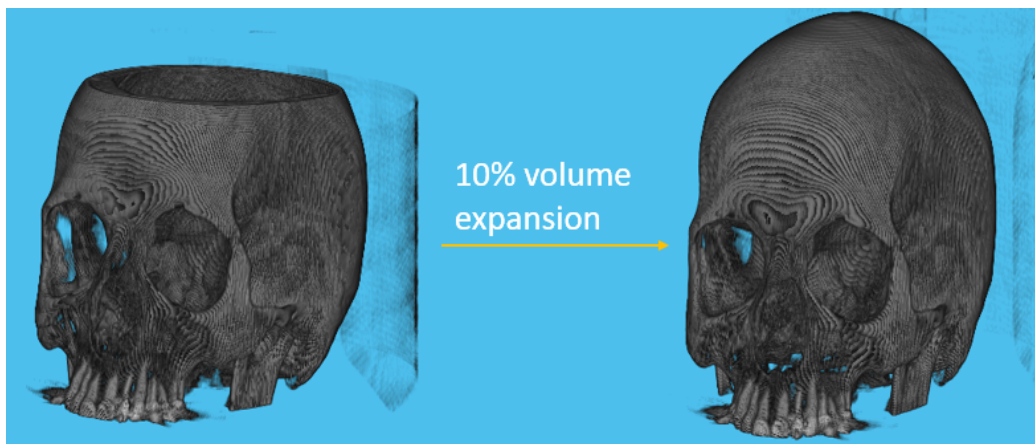

Figure 4.3. Improvement of Sectioning Algorithm with a volume expansion

The following table shows the results obtained on the volumes presented previously with an extension of the Output volume of a value of 10%:

Clinical Case	Section	Template Volume	Sensitivity	Specificity
1	**Femur**	**Other Patient Template**	**100%**	**68%**
1	**Femur**	**Same Patient Template**	**100%**	**85%**
2	Hip	Other Patient Template	98%	75%
2	**Hip**	**Same Patient Template**	**100%**	**83%**
2	Femur	Other Patient Template	98%	75%
2	**Femur**	**Same Patient Template**	**100%**	**92%**

Table 4.2. Sectioning Algorithm Results with a 10% volume expansion

In conclusion the results were excellent in relation to the few and the type of data provided, in fact it was possible to define an algorithm capable of finding and extracting a very specific portion of the volume with fine results, in Figure 4.4 and Figure 4.5 other qualitative results are shown.

Not only was it possible to extract volume portions of a patient thanks to the use of Template volumes obtained from previous CT scans but also thanks to the use of

Template volumes obtained from CT scans of other patients.

This result allows the application of this algorithm even in the case in which the patient approaches for the first time and does not have previous CT scans available.

Figure 4.4. Example of Sectioning Algorithm with hip section.
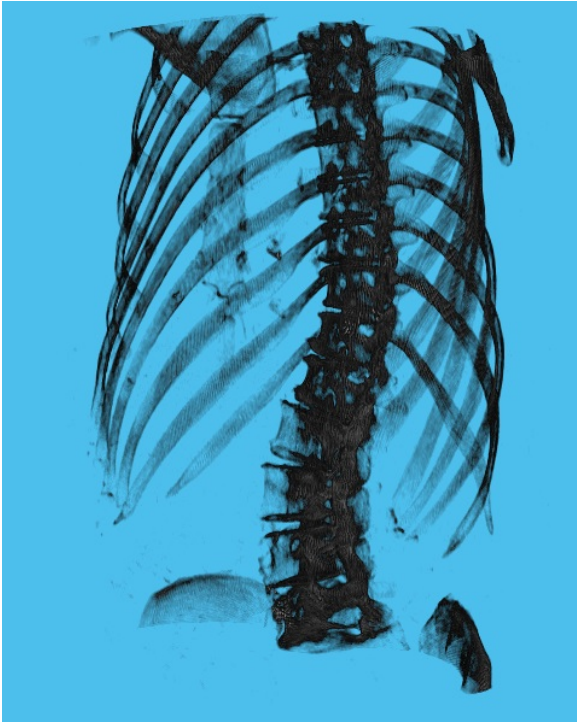

Figure 4.5. Example of Sectioning Algorithm with Rib Cage section.

Another important application of this algorithm is the recognition and automatic extraction of body parts with the aim of building a specific labeled dataset for Multiple Myeloma, this would allow the creation and training of algorithms based on deep learning for further advanced applications.

The process of building a dataset is long and requires a large amount of time, without appropriate technologies to support this process is almost impossible to perform.

To build a specific dataset for Multiple Myeloma it is necessary to operate on a very large quantity of CT scans, for each of these scans the doctor must extract the individual bone sections and provide an appropriate label. Without the support of the Sectioning Algorithm, this process should be performed manually by the doctor, identifying the relevant portions for each scan and extracting the volumes. Thanks to the Sectioning Algorithm, the process could be iterated automatically reducing the time spent by the doctor into the process. To perform the complete work it would be sufficient to provide the algorithm with a series of CT scans as input volumes and the type of section to be extracted. The algorithm automatically extracts the sections from each volume and assigns a label, iterating the process for several sections the only obstacle for the construction of the dataset is the availability of the CT scans itself.

4.2 Alignment Algorithm Results

In this section, the main results obtained with the Alignment Algorithm will be presented. First the results obtained with the application of a threshold to the volumes to be registered to improve the alignment results [4.2.1], then the results obtained by applying the different types of transformation will be discussed [4.2.2].

In order to demonstrate the validity of these processes, several comparisons were made between volumes, to report quantitative data the **Mean Square Intensity (MSI)** of these volumes was calculated.

This value is the average intensity of the voxels and it is related to the spatial dimension of the volumes themselves. This parameter is very useful for comparing parts of the body, especially bone sections. In fact it is an easy to extract index and representative of the volumetric dimension of the bone component, by calculating the MSI of a bone section it is possible to subsequently make evaluations and comparisons with parts of the same section by calculating their MSI.

4.2.1 Thresholding Volumes Approach

In this case we wanted to report and compare the results obtained by thresholding the volumes before the registration process, this process is done to achieve better registration results.

The thresholding process is carried out to exclude the soft tissues of the volume while retaining only the bone structures as shown in Figure 4.6.
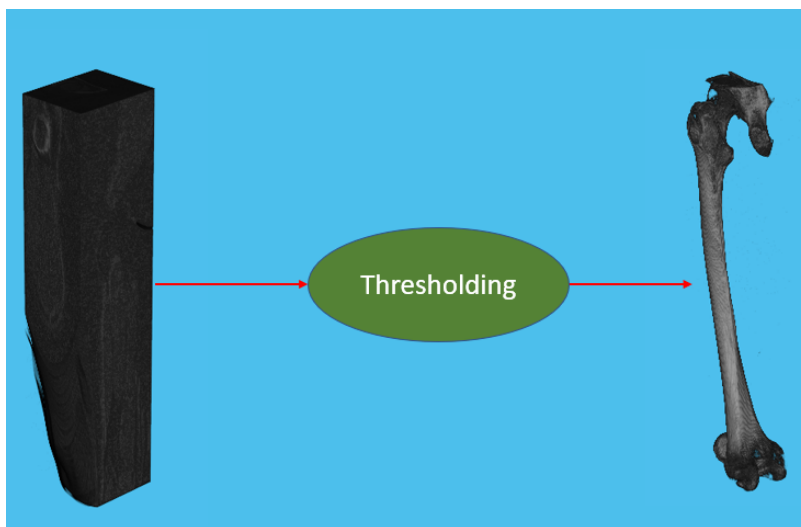

Figure 4.6. Thresholding Result.

This test was conducted in different body parts of all three clinical cases with different resolution and the best results are reported in the Table 4.3.

For descriptive simplicity, the method used on the Right Femur of Clinical Case 1 previously described in chapter 3.1.1 will be reported in the following to demonstrate the workflow of this process as well as the workflow steps are reported in Figure 4.7:

1. Mean Square Intensity of the voxels of the femur from Volume 1.1 was calculated as a Reference of the bone volume (Reference MSI) .

2. the femur Volumes 1.1 and 1.2 were used as input in the Alignment Algorithm without and with the thresholding applied with different values. The application of a threshold involves the extraction of the rigid components present in the volume, in this case the bones excluding the soft tissues..

3. the difference Volume between the femur volume 1.1 and 1.2 after the registration is computed.

4. the Mean Square Intensity of the voxels of the Difference Volume (Final MSI) is computed and compared to the Reference MSI.
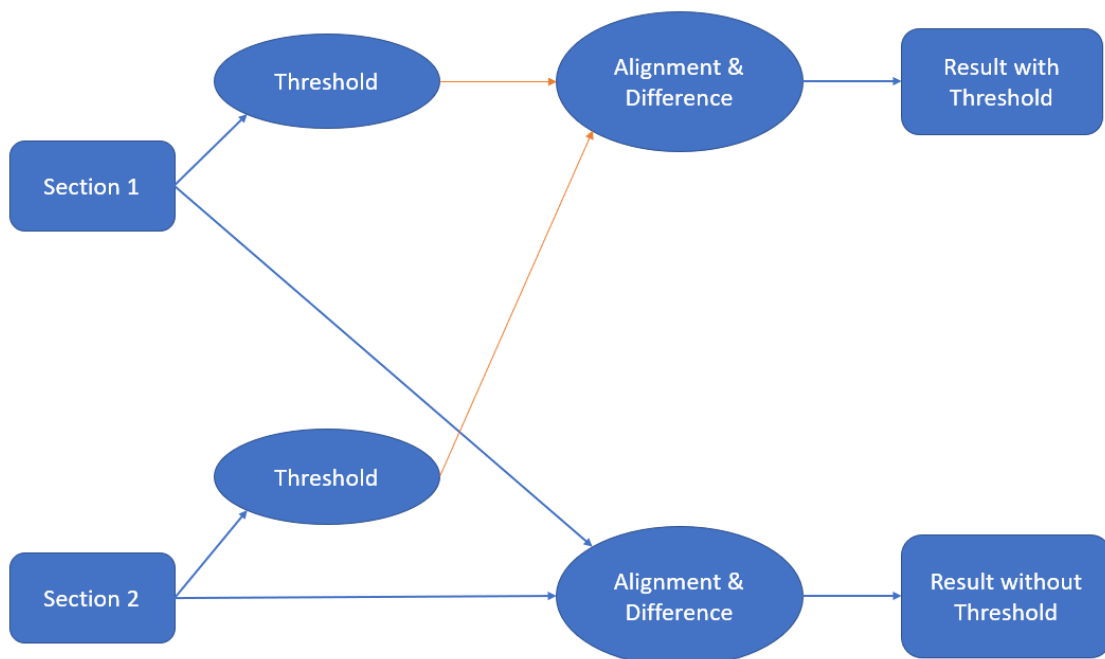

Figure 4.7. Workflow to obtain results on the Thresholding method

In an ideal registration case the Mean Square Intensity(MSI) of the voxels of the Difference Volume will be 0, meaning that the 100% of the voxels are aligned. In our case we already expect a Mean Square Intensity different from zero because of some factor such as moving parts belonging to the examined volume like joints or cartilages. In the Reference MSI column it is reported the MSI of the bone volume taken under examination, in Final MSI column it is reported the MSI of the difference volume which is an estimate of the alignment error, in the Volume Error column it is reported the percentage of volume which is not correctly aligned. It is immediate to evaluate that the application of the thresholding for the volumes has generated a general improvement in the alignment result, in particular in the volume error column

Clinical Case	Section	Threshold	Ref. MSI	Diff. MSI	Volume Error
1	Right Femur	No	0.0218	0.0018065	8.2%
1	Right Femur	0.5	0.0218	0.0003204	1.48%
2	Right Femur	No	0.0172	0.0081	47%
2	Right Femur	0.5	0.0172	0.000523	3%
2	Hip	No	0.0183	0.00026	1.4%
2	Hip	0.5	0.0183	0.00011	0.6%

Table 4.3. Thresholding in Aligning algorithm Results

it is possible to evaluate how the percentage of non-aligned volume is drastically reduced such as in the Right femur of Clinical Case 2 where without the thresholding process the 47% of the bone volume was not correctly aligned and with a thresholding of 50% of the intensity values the bone volume not aligned reduced drastically to 3%.

4.2.2 Transformation Types Evaluation

In this section we want to show which is the best type of transformation to be applied among the possible ones mentioned in the Chapter 2.2.3 and that in our case adding degrees of freedom does not lead to better results.

The difference between two manually extracted bone sections containing the same portions was computed, in this case the difference obtained after alignment is close to zero for each transformation type, this is because of the input volumes were manually sectioned so as to be equal and the difference obtained is ideal. This process is visually reported in Figure 4.8.
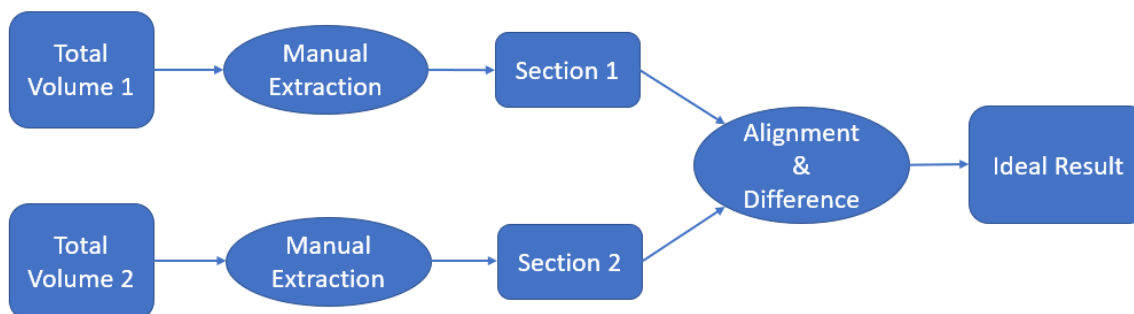

Figure 4.8. Workflow for computing Ideal Results

Quantitative results, reported as the Mean Square Intensity (MSI) of the studied volumes, are shown in the Table 4.4.

Subsequently, one of the two volumes relating to the examined sections is expanded with an additive portion (of a value reported as Additive Volume), through this process we want to simulate an error in the Sectioning Algorithm which, as we have seen, can produce a volume containing portions not belonging to the bone section under examination. With these conditions what we expect as an optimal result is the presence of this additive portion also in the Volume of the Difference, this condition

Clinical Case	Section	Transformation Type	Volume MSI	Difference MSI
1	Humerus	Rigid	0.0034	0
1	Humerus	Similarity	0.0034	0
1	Humerus	Affine	0.0034	0
2	Femur	Rigid	0.0172	0
2	Femur	Similarity	0.0172	0
2	Femur	Affine	0.0172	0

Table 4.4. Results of Alignment with different Transf. Types with controlled inputs

would be the confirmation that the alignment occurs correctly and that the real differences between the two volumes are correctly reported. This process is visually reported in Figure 4.9.

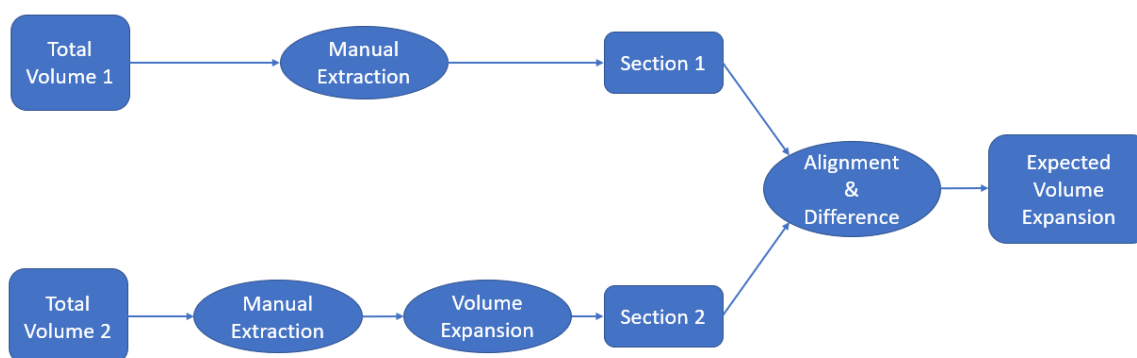Results obtained from the difference with the different types of transformation

Figure 4.9. Workflow for computing the Difference Volume with a Volume expansion added in one of the input sections

applied will be reported below. As reported in the Table 4.5, it can be seen that the

Clinical Case	Section	Transf. Type	Volume MSI	Additive MSI	Difference MSI
1	Humerus	**Rigid**	0.0034	**0.000637**	**0.000637**
1	Humerus	**Similarity**	0.0034	**0.000637**	**0.000637**
1	Humerus	Affine	0.0034	0.000637	0.000495
2	Femur	**Rigid**	0.0172	**0.0074**	**0.00074**
2	Femur	**Similarity**	0.0172	**0.0074**	**0.0074**
2	Femur	Affine	0.0172	0.0074	0.00059

Table 4.5. Results of Alignment with different Transf. Types with different input Volumes

Transformation Types that reported the best results are '**Rigid**' and '**Similarity**' since the *Difference MSI*, i.e. the volumetric portion resulting from the difference of the two aligned volumes, is exactly equal to the *Additive MSI*, i.e. deliberately added volume, demonstrating perfect alignment achieved.

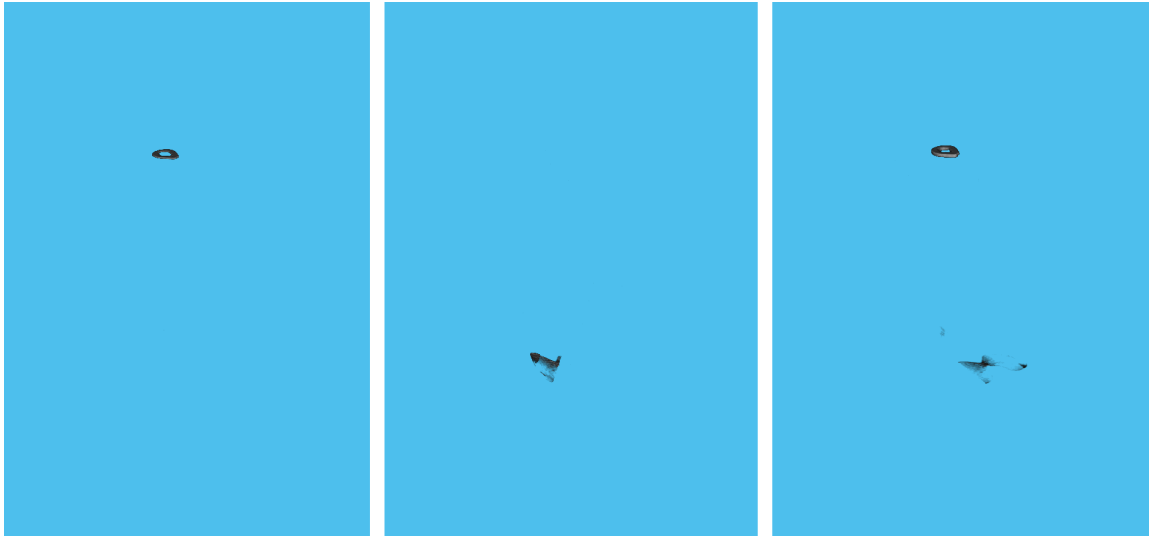It can be noted that the similarity method has further reduced the difference value

67

Figure 4.10. Results of the different alignments between volumes based on the
Transformation Type. Left: *Rigid*; Center: *Affine*; Right: *Similarity*.

MSI, this result, although ideal in order to obtain a final error as low as possible, does not reflect an optimal result in our case. In fact, the final purpose of this algorithm is not to generate a difference close to zero, but to align two volumes in their general structure to highlight the differences, where present.

Further digressions can be made on the choice between rigid transformation and similarity as these two methods produced identical results.

As described in the paragraph 2.2.3, the difference between the two transformations lies in their degrees of freedom, the rigid transformation applies a translation and rotation of the volume while the similarity transformation applies both translation and rotation with the addition of scaling. In our case the volumes have a priori an equal spatial dimension, specified by the step with which the CT scans were performed. In any case, even if the two CT scans to be compared had a different step, a re-sampling of the general volumes would be carried out in previous phases to bring them to same spatial dimensions. With these considerations, therefore, the use of Similarity Transformation is further excluded as scaling would never be applied and adding this degree of freedom would not lead to better results.

In Figure 4.10 it is possible to see visually the difference between volumes obtained with the *Rigid*, the *Affine* and the *Similarity* Transformation type registration. The top portion present in the first and last image is the Additive Volume that is correctly present in the Rigid and Similarity case while it is totally absent in the Affine case.

4.3   Clinical case 1: Femur

In this section the entire proposed workflow applied in a real clinical case will be presented, the parameters used for each step and the results obtained will be displayed. In this case we will examine Clinical Case 1 reported in section 3.1.1, in the medical record provided to us there were lesions recorded in the distal pre epiphyseal site of the right femur.

It is possible in a first moment to evaluate the presence of lesions in the 3d representation of the volume shown in the Figure 4.11 inscribed in the orange circle.
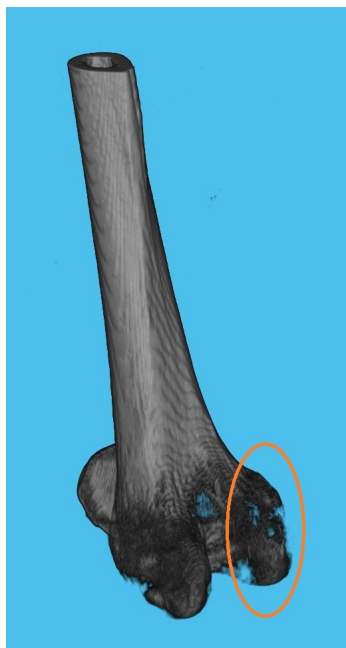

Figure 4.11. Lesions presented in the 3d volume

Later, the extent of the lesion is evaluated with more precision thanks to the Coronal (Y-Z plane), Sagittal (X-Z planes) and Axial (X-Y plane) as reported in Figure 4.12. The lesions in the x, y and z sections are marked in red, a healthy area is marked in blue in order to understand the difference between a lesion and its ideal density. In this case the lesions appear as areas in which the bone is grainy and with a non-continuous surface, it is easy to understand how meticulous the doctor's work is in visually finding these lesions one by one their structure.

Once the lesions have been identified, the doctor then proceeds with the recovery of the patient's CT scans, in this case we have Volume 1.1 and Volume 1.2, acquired one year apart. These two volumes are supplied as input to the Sectioning Algorithm together with a Template Volume, in this case the section of interest is the right femur, therefore a Template Volume of a femur present in the archive is retrieved.

The total volumes used are the high resolution ones, with a spatial size of the slices of 1mm, the 3d volumes have a size of (512,512,1528) for Volume 1.1 and of (512,512,1573) for Volume 1.2.
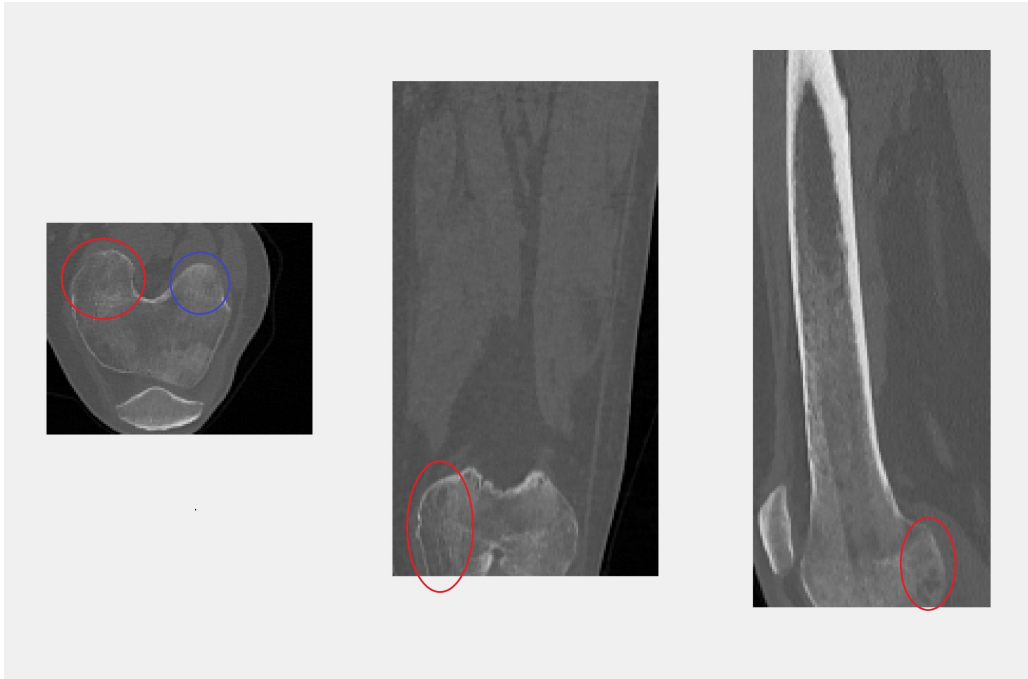
Figure 4.12. Lesions presented in the Coronal, Sagittal and Axial planes

Before being supplied to the Sectioning Algorithm, the volumes are preprocessed with an extraction of the area of interest based on the volume to be searched. In this case we are looking for the right femur so the lower half of the body is dissected by taking the first 754 slices (1528/2) for the Volume 1.2 and the first 787 (rounded 1573/2) slices for the Volume 1.2.

In this case the Sectioning Algorithm used a Rigid transformation with a maximum number of 500 cycles, with a thresholding of the input volumes of the 0.5% of the maximum intensity values and without any resampling.

Once the Sectioning Algorithm has been applied, it will pick up the two femurs from the two total volumes, then a threshold is applied to extract only the bone component of the volumes. These final volumes are shown in section 1 and 2 of the Figure 4.13.
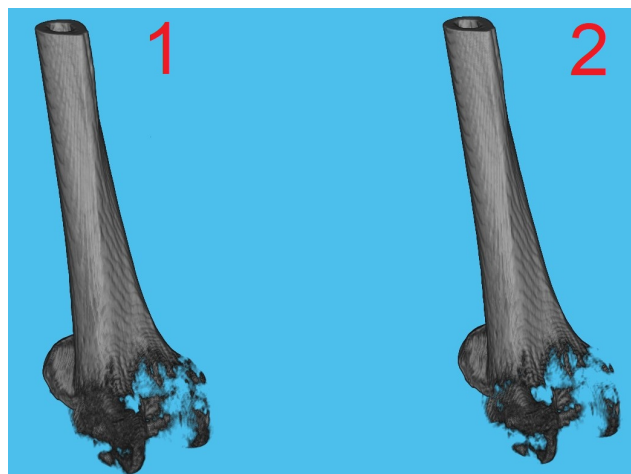

Figure 4.13. Volumes sectioned

The two single sections obtained are then supplied as input to the alignment algorithm, in this case, given the low complexity of the sections, the algorithm has been set with a maximum value of 300 cycles without the use of resampling.

Once the roto-translation matrix has been obtained, this is used to align the two volumes and, once the alignment has been carried out, the difference of the two volumes is produced as shown in Figure 4.14.
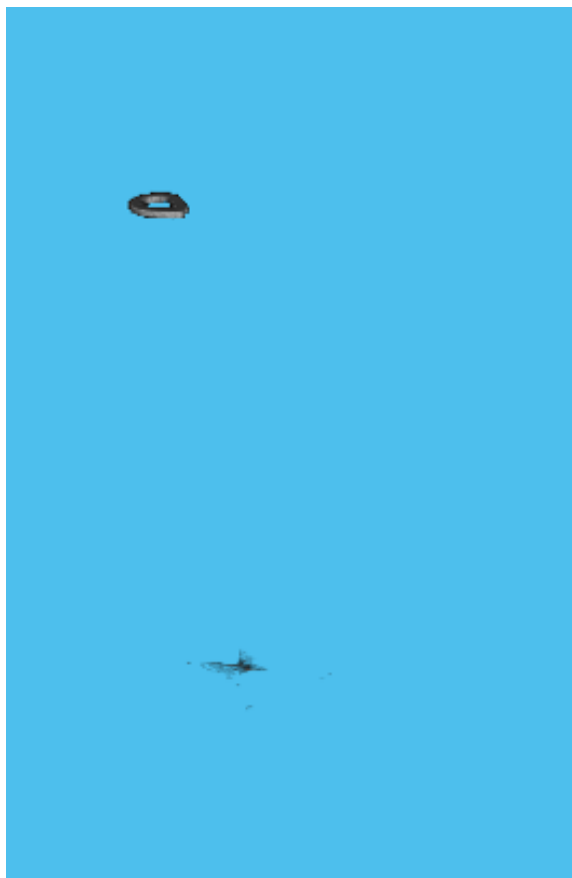

Figure 4.14. Final Difference of femur sections

In this case in the difference volume there is no element in the lesions area to represent that these lesions did develop further in the time span of the two acquisitions.

The only differences between the two volumes are related to a top area of the bone portion, this is because one of the two volumes of the femur included a larger part due to an error in the Sectioning Algorithm output.

The result obtained is therefore a confirmation of the correct alignment and overlapping of the two volumes.

From this overall result it is possible to deduce that in the course of the time passed between the acquisition of the two scans, the lesions relating to this bone portion did not undergo a course but remained stationary.

4.4 Clinical case 2: Head

This section, on the other hand, reports a case in which from the analysis of the difference volumes we are able to find an area of interest.

For this case we started from the medical report which included lesions belonging to the cranium site. In Figure 4.15 is shown the Axial plane of the cranium in correspondence of a portion which could be a bone anomaly such as a lesion described in the blue circle.
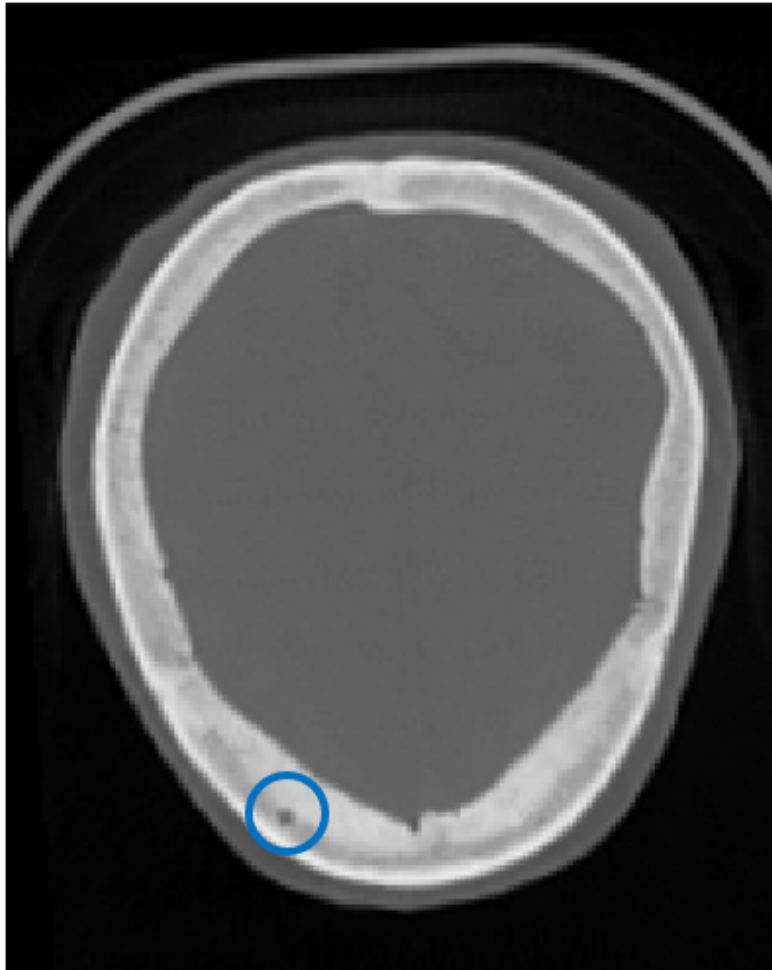

Figure 4.15. Head Lesion reported in the blue circle

Once the lesions have been identified, the doctor proceeds with the recovery of the patient's CT scans, in this case we have Volume 1.1 and Volume 1.2, acquired one year apart. These two volumes are supplied as input to the Sectioning Algorithm together with a Template Volume, in this case the section of interest is the head, therefore a Template Volume of a head present in the archive is retrieved.

The total volumes used are the high resolution ones, with a spatial size of the slices of1mm, the 3d volumes have a size of (512,512,1528) for Volume 1.1 and of (512,512,1573) for Volume 1.2.

Before being supplied to the Sectioning Algorithm, the volumes are preprocessed with an extraction of the area of interest based on the volume to be searched. In this case we are looking for the head so the upper 1/8th of the body is dissected by taking the first 191 slices (1528/8) for the Volume 1.2 and the first 197 (rounded1573/8) slices for the Volume 1.2.

Further processing was carried to the Sectioned Volumes because we are interested in the frontal area of the head, so in order to improve the Alignment result the mandible and part of the maxillary area were removed. This was done because the mandible being a mobile portion could have two different positions in the two acquisitions with respect to the skull, also the removal of the oral cavity with the consequent removal of the teeth improves the process for the same reasons.

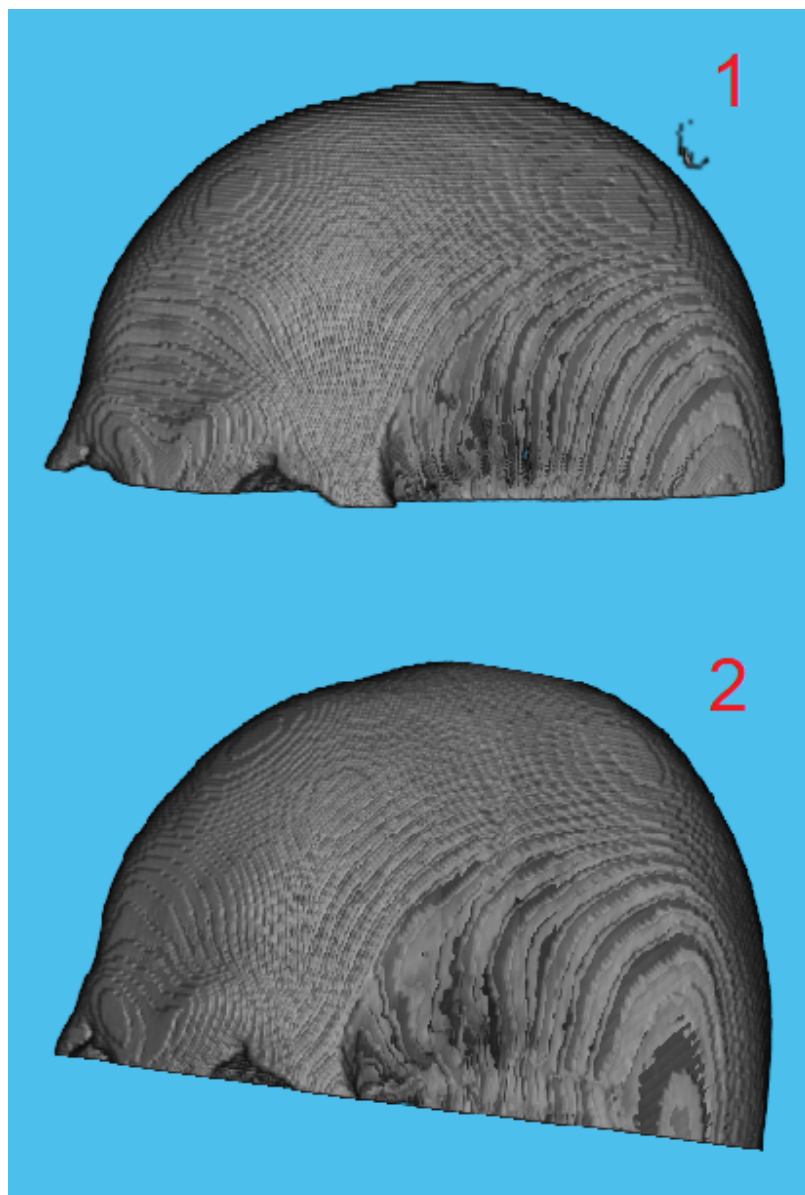The final sectioned Volumes are shown in Figure 4.16.

Figure 4.16. Sectioned Frontal head volumes

The two single sections obtained are then supplied as input to the alignment algorithm, also in this case, given the low complexity of the sections, the algorithm has been set with a maximum value of 400 cycles without the use of resampling.

Once the roto-translation matrix has been obtained, this is used to align the two volumes and, once the alignment has been carried out, the difference of the two volumes is produced as shown in Figure 4.17.
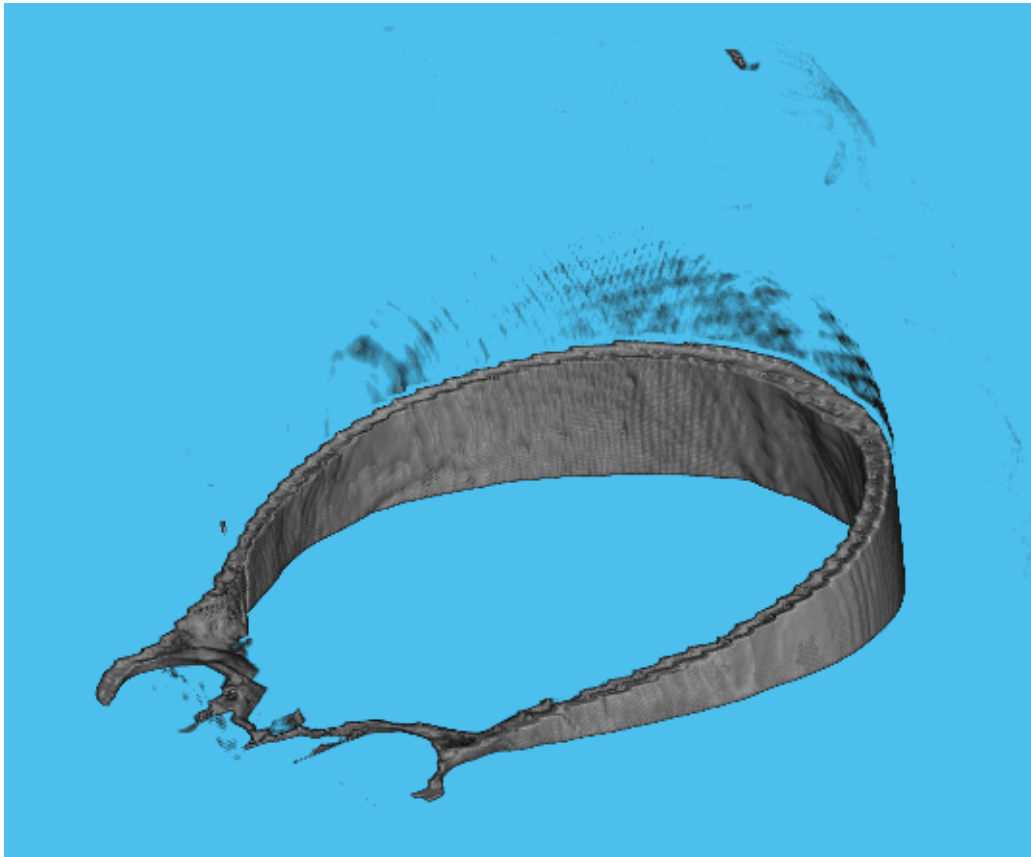

Figure 4.17. Difference of head sections in 3d volumes

In this case it is evident how the position taken by the patient has influenced the Sectioning Algorithm, in fact the volume of the difference shows an area at the base of the volume to indicate that in a CT acquisition the patient has turned his head upwards with respect to to the other CT scan.

This result presented in the volume of the difference, however, is a further confirmation of the precision of the alignment algorithm that has managed to correctly align the most important parts.

In this case in the difference volume there is also an element in the area previously identified to represent that lesions may have developed in the time span of the two acquisitions. This portion is a white area described in Figure 4.18 in the red circle and it correspond to the area where lesions might have developed.

After evaluating the exact position of the area of interest, it was confirmed that this was in the vicinity of the lesions previously found, therefore a thorough study of this area is carried out. In fact, from the metadata it is possible to trace the dimensions in mm of each voxel, in this case 0.97x0.97x0.8mm. So it was possible to accurately calculate the extent of this volume which is approximately 6.77448 mm^3. Finally, it is up to the doctor to carefully evaluate this portion and make further and more in-depth diagnoses. However, this tool has proven effective in finding differences even in very small portions effectively proposing to the doctor areas with a higher priority to be examined.
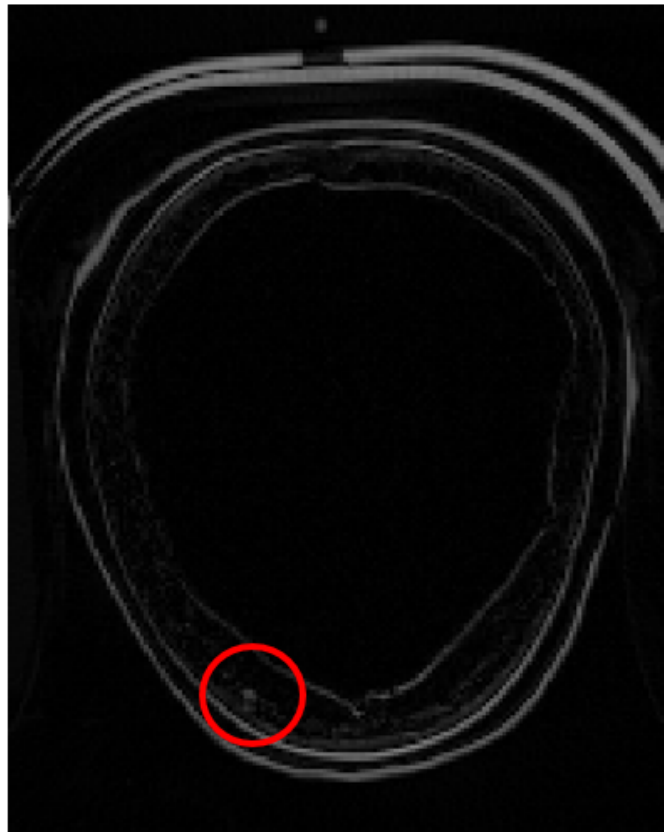

Figure 4.18. Difference of head sections

Conclusions

This thesis work was developed with the aim of creating advanced automatic methodologies to support the physician for the analysis of lesions related to Multiple Myeloma. Even today, technological development in the medical field has not reached all sectors, excluding many rare diseases such as Multiple Myeloma.

The availability of advanced technologies is essential so that the doctor can collect ever more precise data in order to make a correct and accurate diagnosis. The presence of specific tools is essential to facilitate the process of diagnosis and control, tools that must be carefully modeled around the needs of doctors and the nature of the medical condition to be studied.

Currently, only the trained and experienced eye of a specialist doctor can be relied upon to diagnose and monitor developments in patients with Multiple Myeloma. In fact, for this specific condition, there are no specific tools as for other more common diseases and, unfortunately, problems can still exist for which making visual assessments accurately can be difficult even for an experienced doctor. Multiple Myeloma is a type of bone marrow cancer that originates from plasma cells, normally found in the bone marrow, which are cells that are part of the immune system. Multiple Myeloma is a disease that accounts for 1% of all cancers and about 10% of hematological malignancies. It mainly affects adults and elderly people (average age of onset 60 years).

For a correct and in-depth diagnosis it is necessary to identify in the patient the bone lesions typical of Multiple Myeloma, lesions ranging from a size comparable to 1 mm to a larger area and which can affect substantial parts of the bone portion. Given the nature of these lesions, it is very difficult for a doctor to locate and correctly assess the evolution of these lesions over time, this comparison is a fundamental step to evaluate the course of the disease.

This process is obviously limited by several factors such as the experience and the ability of the doctor who operates on the scans, the resolution of the visual support adopted and the size of the lesions that may be imperceptible to the human eye. All these limitations are not only the cause of a final result that can be further improved, but also are the causes of the doctor use of an enormous amount of time due to the repetitiveness of the process especially in high resolution scans.

Furthermore, the process cannot be carried out by any doctor but only by specialized doctors with years of experience

To this end, two main algorithms have been developed that can help the doctor both by reducing the time taken to carry out a total analysis, and by improving the accuracy with which it is possible to identify if a course of the lesion has occurred and to what extent.

These algorithms were designed, optimized and tested by me on clinical cases provided by the National Cancer Institute (INT) simulating a real use case. The ability to develop and test the proposed methods with data such as those provided to us is certainly a great advantage because we were able to simulate real use cases by replicating step by step the work that the doctor should perform.

Furthermore, even the results obtained characteristics are not different from what might occur after the application of these methods in real cases and this confirms the validity of the processes.

The methods developed are aimed at supporting the physician in the phases of sectioning and aligning the volumes so as to be able to evaluate the difference, automating a process that until now must be carried out manually by the physician on each slice of CT scans.

Both methods are based on the application of the co-registration process, a process widely used in image processing. Through co-registration it is possible to align two volumes so as to create a perfect match between the two.

The first method proposed is the sectioning algorithm, this algorithm has the purpose of automatically identifying the sections under examination within total volume scans in order to extract them. This process is of fundamental importance as it allows to focus on subsections so as to improve the accuracy of the studies carried out and speed up the calculation times by working on smaller volumes.

The algorithm receives two volumes as input, the *Total Volume* in which we want to search and a *Template Volume* representative of the area of interest. Through a preprocessing the *Total Volume* is processed to optimize the results based on the area to be searched, in fact a pre-sectioning is carried out using the proportions of the human body as a guide. For example, if the point of interest is the head, the first 1/8 in the z-axis of the volume is extracted.

Other preprocessing carried out on the volumes are *Resampling* and *Thresholding*, the former being carried out to exploit the *Coarse-to-fine* process where necessary. This provides for the resampling of very large volumes to reduce the dimensionality and therefore facilitate the calculation times of the subsequent processes, once the results are obtained, they are remapped on the dimensions of the original volumes and applied to them.

In this way, high resolution results are obtained by exploiting low resolution volumes to carry out processes.

The second preprocess carried out is the application of thresholding, this process allows to extract only the most significant components of the volumes such as the bone parts excluding the soft tissues, in fact the latter are not suitable for comparing two volumes as they can undergo radical changes over time. Spent between the two CT scans acquisitions thresholding therefore improves the general results obtained by making both sectioning and alignment processes more precise.

The *Template Volume* can be extracted from a CT scan of the same patient available or it can be a generic template volume belonging to another patient, in fact good results have been obtained with both types of volumes and thanks to the use of a degree of expansion of the volumes also the results obtained with generic templates, previously lower, have reached satisfactory levels.

The *Alignment Algorithm*, on the other hand, aims to align two volumes belonging to different scans of the same patient and then make the difference. The volumes

supplied as input are two body portions obtained from two different CT scans of the same patient, for example two femurs or two pelvises. This is because through the algorithm with two scans carried out one or more years apart, we will be able to assess whether in specific areas where lesions have been appropriately identified these have undergone a significant course.

At first the Sectioning Algorithm is used to extract from two CT scans of the same patient carried out in different years the same bone portion where a lesion caused by Multiple Myeloma has been identified, subsequently these two portions are suitably processed with a resampling or a thresholding discussed above. Once these portions have been extracted, they are aligned with a co-registration process suitably optimized based on the size of the volumes, the available computing power and the desired accuracy.

Once the volumes are aligned, their difference is produced and a graphic representation developed, in this case the areas where there are differences will be easily identifiable. If in the areas of the volumes of the differences in which lesions were found, the presence of any portion is evaluated then this is examined as it could represent a course of the lesions themselves.

Thanks to the use of the metadata provided with the CT scan files it is possible to calculate the volume of these areas and in which direction they have developed, all this information will be useful to the doctor to evaluate the speed with which Multiple Myeloma develops and also the direction where lesions are developing so as to predict and prevent further compromise of the affected bones.

The results of all proposed methods have been verified and reported, in general the validity of the algorithms has been verified and it has been demonstrated how they could be substituted for the current manual methods followed by doctors.

In fact, two complete cases of use have been reported, the first without evidence of injury developments and the second with evidence of an area of interest. In the second case, a clinical case study was developed by analyzing the extent of lesion growth.

However, both the sectioning algorithm and the alignment algorithm found a performance reduction when the volumes under examination had particularly compromised or complicated conformations, specifically areas with multiple levels of mobility such as the head with the mandibular appendix or the hands with finger components.

This shows that it is not possible to generalize the application of the methods to all parts of the body and the presence of an operator to optimize and rectify the processes is still a necessary condition. The results obtained, however, are not algorithms capable of making diagnoses, but are only tools at the service of the doctor to facilitate the patient's study and diagnosis process.

The possibility of extending these methods with deep learning algorithms able to classify and make decisions is not excluded in the future, at the moment it was not possible to proceed in the development of systems on artificial intelligence since it was not possible to recover a suitably labeled dataset containing volumes specific with bone lesions typical of Multiple Myeloma. For this purpose, one of the two proposed methods, the sectioning algorithm, can also be used to facilitate the construction of this data set. The process of building a data set is long and requires a large amount of time and for this reason having an algorithm suitable for this purpose is essential, in fact with the proposed sectioning algorithm the only limit is availability CT scan as it automates every aspect of the component extraction and labeling process.

This thesis work was developed in the year we really realized how important in the medical field research and development is. The development of specific and optimized methods for certain pathologies does not exclude the possibility of extending the field of application. For this reason this thesis proposes the purpose and the hope that it can be a first step towards the development of solutions that can one day make a difference.

Bibliography

[1] [Online]. Available: myeloma.org/pdfs/PH2011-Ital_a1.pdf

[2] L. W. Nau, K.C., "Multiple myeloma: diagnosis and treatment," 2009.

[3] [Online]. Available: https://www.cancer.org/acs/groups/cid/documents/ webcontent/003121-pdf.pdf

[4] B. Zitova and J. Flusser, "Image registration methods: a survey," *Image and vision computing*, 2003.

[5] M. Kourogi, T. Kurata, and K. Sakaue, "A panorama-based method of personal positioning and orientation and its real-time applications for wearable computers," in *Proceedings Fifth International Symposium on Wearable Computers*. IEEE, 2001.

[6] A. Habib and R. Al-Ruzouq, "Semi-automatic registration of multi-source satellite imagery with varying geometric resolutions," *Photogrammetric Engineering & Remote Sensing*, 2005.

[7] K. Yano and I. Kumazawa, "A modified nearest neighbor method for image reconstruction in fluorescence microscopy," in *International Conference Image Analysis and Recognition*. Springer.

[8] G. Dedeoglu, T. Kanade, and S. Baker, "The asymmetry of image registration and its application to face tracking," *IEEE transactions on pattern analysis and machine intelligence*, 2007.

[9] J. A. Maintz and M. A. Viergever, "A survey of medical image registration," *Medical image analysis*, 1998.

[10] H. IH, "Mitchell kd. mulem rv. barnes pd, trãªvesst. registration and alignment of three-dimensional images: an interactive visual approach," 1996.

[11] P. Besl and N. Mckay, "A method for registration of 3-d shapes, ieee trans." *P flattern Anal. and M ac h ine I ntell*, 1992.

[12] W. Zhao, T. Y. Young, and M. D. Ginsberg, "Registration and three-dimensional reconstruction of autoradiographic images by the disparity analysis method," *IEEE Transactions on medical imaging*, 1993.

[13] A. Andronache, P. Cattin, and G. Székely, "Local intensity mapping for hierarchical non-rigid registration of multi-modal images using the cross-correlation coefficient," in *International Workshop on Biomedical Image Registration*. Springer, 2006.

[14] D. Mattes, D. R. Haynor, H. Vesselle, T. K. Lewellen, and W. Eubank, "Pet-ct image registration in the chest using free-form deformations," *IEEE transactions on medical imaging*, 2003.

[15] C. E. Shannon, "A mathematical theory of communication," *The Bell system technical journal*, 1948.

[16] C. A. Pelizzari, G. Chen, D. R. Spelbring, R. R. Weichselbaum, and C.-T. Chen, "Accurate three-dimensional registration of ct, pet, and/or mr images of the brain." *Journal of computer assisted tomography*, 1989.

[17] D. L. Hill, P. G. Batchelor, M. Holden, and D. J. Hawkes, "Medical image registration," *Physics in medicine & biology*, 2001.

[18] J. V. Hajnal and D. L. Hill, *Medical image registration*. CRC press, 2001.

[19] P. Thompson, "Mega ms. woods rp. zoumalan ci. lindshield cj. blanton re. moussai j. holmes cj. cummings jl. toga aw. cortical change in alzheimer's disease detected with a disease-specific population-based brain atlas," *Cerebral Cortex*, 2001.

[20] J. Zhang and A. Rangarajan, "Affine image registration using a new information metric," in *Proceedings of the 2004 IEEE Computer Society Conference on Computer Vision and Pattern Recognition, 2004. CVPR 2004.* IEEE, 2004.

[21] S. Wright and J. Nocedal, "Numerical optimization," *Springer Science*, 1999.

[22] G. E. Christensen, R. D. Rabbitt, and M. I. Miller, "Deformable templates using large deformation kinematics," *IEEE transactions on image processing*, 1996.

[23] [Online]. Available: https://it.wikipedia.org/wiki/DICOM

[24] [Online]. Available: https://www.mathworks.com/matlabcentral/fileexchange/53745-medical-image-reader-and-viewer